Research Square

Preprints are preliminary reports that have not undergone peer review.
They should not be considered conclusive, used to inform clinical practice,
or referenced by the media as validated information.

Distal airway-specific condensation of saliva-free exhaled aerosols enables quantification of pulmonary SARS-CoV-2 RNA load in early COVID-19

John Henderson
Northumbria University
Theodora Mantso
Northumbria University
Saqib Ali
Northumbria University
Rüdiger Groß
Ulm University Medical Centre
Janis A. Müller
Ulm University Medical Centre
Amie Wilkinson
University of Westminster
Louise Usher
University of Westminster
Beth Auld
University of Sussex
Anil Namdeo
Northumbria University
Madeleine Combrinck
Northumbria University
Phil Hackney
Northumbria University
Volkan Turgul
University of Westminster
Edison Jahaj
National and Kapodistrian University of Athens
Nikolaos Athanasiou
National and Kapodistrian University of Athens
Taxiarchis Nikolouzakis
University of Crete
Pedro J. Almeida
Federal University of Minas Gerais
Chrysa Rokka

National and Kapodistrian University of Athens
Daniel C. Queiroz
Federal University of Minas Gerais
Edward Wright
University of Sussex
Alexandros Zafiropoulos
University of Crete
Izzet Kale
University of Westminster
Diamantis P. Kofteridis
University Hospital of Heraklion
Aristides Tsatsakis
University of Crete
Jan Münch
Ulm University Medical Centre
Michelle A. Sugimoto
PulmoBioMed Ltd, Newcastle Upon Tyne
Paraskevi A. Katsaounou
National and Kapodistrian University of Athens
Anastasia Kotanidou
National and Kapodistrian University of Athens
Pagona Lagiou
Federal University of Minas Gerais
Gkikas Magiorkinis
National and Kapodistrian University of Athens
Renato S Aquiar
Federal University of Minas Gerais
Mauro M. Teixeira
Federal University of Minas Gerais
Sterghios A. Moschos
sterghios.moschos@northumbria.ac.uk

Northumbria University

Research Article

Keywords: Exhaled breath condensate, respiratory aerosols, SARS-CoV-2, COVID-19, resource-limited settings

Posted Date: April 28th, 2026

DOI: https://doi.org/10.21203/rs.3.rs-9463976/v1

License: This work is licensed under a Creative Commons Attribution 4.0 International License. Read Full License

Additional Declarations: Competing interest reported. Prof. Moschos and Prof. I. Kale co-invented PBM-Hale™ (patent no. WO2017153755). Prof. Moschos, Prof. Kale, Dr. Torgul, and Northumbria University are shareholders to the Northumbria University spinout company PulmoBioMed Ltd. Prof. S. A. Moschos, Dr. M. A. Sugimoto, and Mr. S. Ali are employees of PulmoBIoMed Ltd. All other authors declare no competing interests.

Abstract

Rationale:

Condensation of exhaled breath promises a non-invasive alternative to sampling epithelial lining fluid (ELF) from the small airways. Clinical adoption is hampered by poor sampling reproducibility, biomarker level inconsistencies, and saliva contamination.

Objective

We evaluated a novel, hand-held collector, designed for distal lung fluid capture in self-sealing containers, for quantifying lower respiratory tract infection (LRTI) load.

Methods

Exhaled breath condensate (EBC) specimens were collected via tidal breathing or singing. Sampling reliability was determined in healthy participants, by salivary α-amylase and 18S ribosomal RNA (rRNA) assays. Immunoassays for alveolar surfactant protein D (SP-D) and inflammatory cytokines quantified the impact of exhalation maneuvers on breath condensate protein content. Matched nasopharyngeal swabs, saliva, and EBC were collected in primary care and hospital ward pilot studies. Diagnostic nucleic acid amplification test quantified human and viral RNA load in the first 5 days from COVID-19 symptom onset.

Measurements and Main Results:

Salivary amylase-free sampling was linear (R^2 = 0.9995; 0.25-30 min), containing proportional and consistent amounts of eukaryotic 18S rRNA, but undetectable human GAPDH, RNase P, or beta actin mRNA. Preferential condensation of end-expiration aerosols was confirmed by ~ 2 log higher SP-D levels vs cytokines, irrespective of exhalation mode. SARS-CoV-2 RNA genomes were detected only by singing for >2min in 100% of COVID-19 cases in the first 5 days from symptom onset. 18S rRNA normalization revealed 85x higher viral RNA loads in the lung vs paired saliva and not correlated to nasopharyngeal loads.

Conclusions

The non-invasive PBM-Hale™ EBC collector reproducibly and robustly samples saliva-free ELF to specifically inform pathogen levels in the distal airways.

Background

Air expelled from the lungs becomes humidified by water vapour and fluid lining the respiratory tract epithelium, as well as the oral and nasal epithelium, by means of the ‘fluid film burst’ mechanism [1], resulting in aerosols released as a component of exhaled breath. These dry and aqueous particles are predominantly

fine aerosol (FA) particles by number, as well as large droplets (LD), which instead dominate by mass [2]. Fine aerosols originate from distal airways and alveoli, while most LD production is physically restricted to the upper airways and oropharyngeal epithelium; LD generated in distal regions during exhalation are efficiently deposited by inertial impaction along the respiratory tree branchings and the 90° pharyngeal bend [3].

Upon exhalation, both particle types can remain airborne contributing to infectious respiratory particles [4], depending on air movement, ambient temperature, and relative humidity [5]. Environmental physical parameters drive particle size evolution: hydration-driven swelling leads to gravitational sedimentation, whereas evaporative shrinking drives extended airborne diffusion [6]. Capture and analysis of exhaled FA proximally to the mouth therefore offers the unique opportunity to specifically analyse biomarkers originating from the lower respiratory tract, provided cross-contamination with upper respiratory or oral droplets is prevented. Such a solution could potentially substitute invasive methods e.g. tracheal aspirates and bronchoalveolar lavage (BAL), or potentially infectious aerosol-generating sputum induction; methods inherently subject to contamination from the mouth and upper respiratory tract.

Cooling exhaled breath [7–11] yields a condensate of respiratory gases, aerosols, and droplets collectively known as exhaled breath condensate (EBC). The resulting aqueous sample can be analysed by Enzyme-Linked Immunosorbent Assay (ELISA), western blotting, Reverse Transcription Polymerase Chain Reaction (RT-PCR), mass spectrometry, among other analytical techniques. Beyond viral and bacterial infections, analysis of EBC has revealed differential levels of cytokines, growth hormones, lipids, microRNAs, distinct metabolomic profiles and volatile organic compound (VOC) signatures, associated with a range of pathological states: lung cancer [12, 13], pulmonary fibrosis [14, 15], bronchoconstriction [16], physiological shock [17] and even neurological disorders [18].

Despite the promise of EBC, clinical adoption has been restricted to VOC gas mass spectrometry for the detection of *Helicobacter pylori* gastric infection [19]. Challenges beyond this indication centre on the poor reliability of EBC collectors [3, 20]; thus, in 2005 [20] and again in 2017 [3], Horvàth *et al.* highlighted key technical issues regarding EBC collection, and the need to establish consistent practices for collection and analysis. Specifically, challenges were identified in i) saliva and environmental EBC contamination, ii) EBC sampling reproducibility, iii) condensation temperature stability, iv) flexibility that guarantees detection of markers with varied thermal sensitivities, and v) optimized specimen capture for peripheral airway content [3].

Until the emergence of COVID-19, limited progress had been made in solving these problems. Indeed substantial unmet need remains in accurately diagnosing and identifying the causal agent to enable targeted treatment of acute lower respiratory tract infections [21], improving diagnosis and treatment of chronic respiratory diseases [22], or mitigating the persistent threat of aerosolized bioweapons [23]. To date, breath diagnostics have predominantly focused on exhaled VOC analysis [24–28]. Nonetheless substantial diagnostic value remains in directly identifying the causal agents of infectious diseases and non-volatile inflammatory host biomolecules in exhaled aerosols.

We hypothesized that a proximal inertial saliva trap, coupled to an exhalation flow path favoring small airway-derived FA condensation, in a configuration that returns EBC specimens in a sealed container, could help overcome the challenges to EBC adoption in clinical diagnostic workflows. The aims of this study were i) to evaluate if such a device can isolate distal lung FA EBC free of saliva, and ii) to inform viral loads specific to

the distal lung in the context of the COVID-19 pandemic, and reports of SARS-CoV-2 in exhaled breath. Building upon findings of higher SARS-CoV-2 RNA emission during singing, we show our novel FA EBC specimen collector favours viral load quantification specifically in the lower airways, particularly when a singing maneuver is applied. We confirm by molecular testing 85-fold higher lower respiratory viral levels after normalisation compared to saliva, independent to nasopharyngeal swab levels, with high percent positive agreement to nasopharyngeal swab detection.

Methods

Participant Recruitment

Research with human participants was performed in accordance with the Declaration of Helsinki. All healthy volunteer EBC samples were obtained with participant informed consent under Northumbria University ethics application no. 43341 approved by the Department of Applied Sciences Subcommittee of the University Research Ethics Committee. All COVID-19 patient EBC samples were collected with informed consent under the National and Kapodistrian University of Athens General Hospital 'Evangelismos' ethics application protocol no. 280/24-4-2020 approved by the Scientific Committee of the General Hospital 'Evangelismos' and approval no. 54358021.1.0000.5149 by the Institutional Review Board of the Federal University of Minas Gerais. Patients in Greece were recruited among attendees of the Emergency Department of Evangelismos Hospital, Athens, Greece, and the University General Hospital of Herakleion, Herakleion, Crete, Greece, between June 2020 and June 2022. The cohort included hospitalized patients who were either convalescent and nasopharyngeally negative for SARS-CoV-2 (n = 2; week 3 post-symptom onset) or within the first 5 days of hospitalization (n = 10; >2 weeks post-symptom onset). In the second phase, 30 acutely symptomatic patients with nasopharyngeal swab (NPS)-confirmed SARS-CoV-2 infection were enrolled.

In Brazil, patients were recruited from the suburban primary care centre 'Centro de Saúde Jardim Montanhes', Center for Advanced and Innovative Therapies, Federal University of Minas Gerais (Belo Horizonte, Minas Gerais), between March and July 2022. Participants were included in the study if acutely symptomatic for COVID-19 (days 0–5 from symptom onset, symptoms consisting of fever, persistent cough, dysgeusia or dysosmia, or dyspnoea) and confirmed positive for SARS-CoV-2 by NPS lateral flow test.

EBC Sampling Devices

Custom components of the novel EBC collector (PBM-Hale™, WO2017153755; Fig. 1) were produced in-house and decontaminated as described in the Supplementary Methods. The device comprises of a saliva-trapping separator with a one-way inspiratory valve to prevent inhalation through the device and a 50 mL EBC specimen collection vessel with a self-sealing platform lid (Fig. 1A). Upon assembly, the specimen vessel is unsealed by interfacing with the separator (Fig. 1B). The separators' internal architecture was designed to promote turbulent inertial impaction during sampling to remove saliva-containing LD from exhaled breath. FA not subject to inertial impaction flow through the 50mL EBC specimen vessel via a first port, and out via a second port into the separator exhaust compartment, and then onto the environment. The EBC collection vial is fitted with a self-sealing platform lid designed to contain the EBC specimen in the specimen vessel while

preventing ambient aerosol contamination and EBC evaporation, protecting specimen integrity and operator safety. Condensation temperature was controlled using a custom-built Coolant Chamber enabling collection at room temperature, 0°C (wet ice), or − 78.5°C (dry ice).

Computational Flow Modelling and Experimental Testing

Computational flow and thermal modelling were executed in Solidworks v. 2021sp3 using a tidal breath flow model of 95% relative humidity exhaled breath at 35^{o}C, 0.5L/3sec laminar flow. The duty cycle model employed [29] [30] had a 5sec period; expiration was modelled at 0.2L/sec, 0.15l/sec, 0.15L/sec flow for each of the first 3 seconds of each breathing cycle, followed by 0L/sec flow for the 2sec inspiration phase reflecting the inhalation prevention valve function in PBM-Hale™. Flow and temperature calculations were computed as described in the Supplementary Methods. Device temperature was monitored using a Mastech MS6514 probe thermometer fitted with a type T thermocouple (Amazon, London, UK). Airborne particle size was measured with a Particles Plus® 8506 Handheld Particle Counter fitted with a Particles Plus® temperature and humidity probe (Particles Plus, Inc., Stoughton, MA).

FA EBC, LD, and Saliva Specimen Collection

EBC specimens were obtained by tidal oral breathing for the indicated time, or by singing as loudly as possible “happy birthday” in Portuguese for up to 15min per Coleman *et al*. [33]. The Cooling Chamber was filled with powdered dry ice, commercially procured dry ice pellets (~ 1x3cm), or crushed wet ice. Coolant was replenished every 30 minutes during sampling. The PBM-Hale™ was exposed to the environment just before initiating sampling and immediately isolated upon sampling completion. The separator was locked onto the coolant chamber and the inner separator part (blue component in Fig. 1A) actuated into the armed position by pressing down only immediately prior to initiating sampling, and after removing the separator inlet and outlet foil covers (Fig. 1A). Interruptions during sampling (e.g. coughing, speaking, removal from the device) were recorded and expressed as the number of interruptions per sampling period for subsequent correlation analyses. After sample collection, the inner separator was returned to the unarmed position, and then unloaded; two motions that physically isolated LD within the separator, and returned the custom platform lid into the closed position isolating the FA EBC (yellow tab in Fig. 1A). Samples were placed on wet ice before centrifuging at 4,000xg for 1 minute to pool the EBC at the bottom of the 50mL tube. Sample volumes were quantified using Sartorius Picus electronic single channel pipettes equipped with RNAse/DNase free barrier tips (Sartorius UK Ltd., Epsom, UK). The sample was then either immediately processed or stored at -80°C. The LD fraction was removed from PBM-Hale™ by syringe and needle puncture of the saliva trap-containing separator. Saliva samples were collected by drooling for 2 minutes into a microcentrifuge tube, centrifuged at 4,000 × g for 1 minute, and supernatants collected for analysis.

Protein analysis

EBC specimens were lysed using RIPA buffer, and the protein concentration was determined by a micro BCA assay (ThermoFisher) as described in the Supplementary Methods. The FA and LD fractions of EBC

specimens, or fresh saliva samples subjected to a freeze-thaw cycle on dry ice (diluted 1:200 with physiological saline), were analysed using an α-amylase kinetic assay (Salimetrics LLC, Carlsbad, CA) following the manufacturer's protocol. Cytokine concentrations were determined by a MesoScale Discovery's V-Plex assay (healthy specimens) or a MILLIPLEX® MAP Luminex® human cytokine/chemokine magnetic bead panel (Merck; HCYTOMAG-60K; COVID-19 specimens), according to the manufacturer's instructions.

RT-PCR

For PBM-Hale™ prototype testing RNA was extracted with TRIzol (Thermo Fisher Scientific), quantified by UV spectrophotometry, and subjected to two-step RT-PCR as described in the Supplementary Methods.

Volumes of 0.2mL (NPS) or up to 1mL (FA EBC) of clinical samples collected in Greece were RNA extracted using the Complex800_V6_DSP protocol with the QIAsymphony DSP/Pathogen Midi kit (SafeBlood BioAnalytica SA, Athens, Greece), eluting 0.06mL. SARS-CoV-2 RNA load was quantified using the VIASURE SARS-CoV-2 (ORF1ab and N genes) Real Time PCR Detection kit at a manufacturer's analytical limit of detection of 10 target copies per reaction (5μl RNA extract in a 20μl reaction; CerTest Biotec, Zaragoza, Spain), using the internal control at a ratio of 0.1μl internal control/μl eluate. All samples were analysed in single reactions and viral load was expressed as the average threshold cycle (Ct) of the positive targets per sample.

For maximal sensitivity to SARS-CoV-2 detection in the cohort sampled in Brazil, the whole FA EBC volumes collected were submitted to RNA extraction using PureLink™ RNA Mini Kit, Invitrogen™ (Carlsbad, CA, USA); final elution volumes were 30μl. Volumes of 2μl were then assayed by real time RT-PCR in 10μl reactions containing iTAQ Universal Probes One-Step Kit, Bio-Rad Laboratories (Hercules, CA, USA) supplemented with pan-eukaryotic 18S rRNA Taqman® primer/probe mix (Thermo Fisher) or the multiplexed CDC SARS-CoV-2 assay (Integrated DNA Technologies Inc., Coralville, IA, USA), targeting two different regions of the viral nucleocapsid gene (N1 and N2 [34]) vs human RNase P. Reactions were carried out in technical triplicates (20% of total sample RNA extract or 3min of sampling via singing and 6min of sampling via tidal breathing) to increase the chances of detection [35, 36]. Ct's for each target were calculated as the average of three technical replicates (± standard deviation) with SARS-CoV-2 Ct's defined as the average Ct's of the two targets. Fold-differences were calculated based on the $2^{-\Delta\Delta Ct}$ method.

Recombinant virus, virus-like particle, and nanoparticle nebulization assays

Lentivirus encoding Green fluorescent protein (GFP), pseudotyped with vesicular stomatitis virus (VSV) glycoprotein (VSV-GFP), rabies virus (RABV), and D614G Beta SARS-CoV-2 were produced as previously described [37]. Infectious virus concentration was determined by fluorescent cell sorting (BD FACSCanto™ II, BD Biosciences, Wokingham, UK) for GFP [38] and as described in the Supplementary Methods. Polystyrene (PS) flurosphere beads (100nm diameter 505/515 fluorescence FluoroSpheres) were obtained from ThermoFisher. Liposomes were produced by synthetic lipids (Avanti Polar Lipids, Alabaster, AL, USA) using thin-film hydration and extrusion as previously described [39]. Lipid composition was either 99 mol% dioleoylphosphatidylcholine (DOPC; neutral liposomes) or 49 mol% DOPC and 50 mol%

dioleoylphosphatidylserine (DOPS; negative liposomes), in each case including 1 mol% TopFluor-phosphatidylcholine (PC) to enable detection by fluorescence nanoparticle tracking analysis (NTA). Lentiviral virus-like particles (VLPs; MLVgagYFP-VLPs) and SARS-CoV-2-VLPs were prepared as previously described [40, 41]. Nanoparticle suspensions diluted in cell culture media, physiological saline, or deionized water were nebulized for 5-15min using a PARI Turboboy SX or PARI Boy Classic (PARI Medical Ltd., Byfleet, UK). These devices generate aerosols with a mass median diameter of 3.5μm wherein 67% of the mass is in particles <5μm. Aerosols were routed directly into PBM-Hale™ using a custom 3D-printed polylactic acid adapter. Nanoparticle size, zeta potential, and concentration were determined using a ZetaView TWIN (ParticleMetrix GmbH, Inning am Ammersee, Germany), at 480nm with the exception of SARS-CoV-2-VLPs, which are not tagged and were analyzed in scatter mode. Nebulised VSV-GFP infectivity was determined in HEK-293T cells as described in the Supplementary Methods.

Statistics

Statistical analyses were carried out in GraphPad Prism v10.6.1 (GraphPad Software, San Diego, CA). Sampling consistency was determined by plotting sample volumes over time and performing regression analyses after anchoring Y axis intercepts to zero and computing the probability of regression slope difference. Differences in particle concentrations and analyte levels were compared by ANOVA followed by post hoc tests for pairwise comparisons (Tukey multiple comparison tests for low replicate virological and qPCR experiments (n = 3–5) with limited variable analysis, and Holm-Šídák multiple comparisons for large replicate (aerosolized particle count and NTA) experiments). Paired comparisons were analysed using paired t-tests or Wilcoxon matched-pairs signed-rank tests, as appropriate. Group comparisons were analysed using Kruskal–Wallis tests followed by Dunn's multiple comparisons test or paired 1-way ANOVA. Correlations were assessed using non-parametric Spearman analysis.

Results

PBM-Hale™ linearly captures saliva-free fine aerosols enriched for distal lung protein biomarkers

Since gas-phase water condenses on particles at low temperature, we hypothesised that operating PBM-Hale™ below room temperature would induce condensational growth of fine aerosols and enhance their capture in the collection vial. To test this, we measured particle counts at the breath collector exhaust during 3 minutes of tidal breathing at room temperature (r.t.), or 0°C (wet ice) and − 78.5°C (dry ice) cooling. Compared with room temperature, dry ice had the strongest effect on aerosol growth, with statistically significant depletion of ultrafine particles (< 0.3 μm; Supplementary Fig. 1A) and enrichment of larger particle sizes (0.5–10 μm; Supplementary Fig. 1C-F). Wet ice also reduced the number of < 0.3 μm particles and increased the counts of 1–5 μm particles but did not affect 0.5-1.0 μm or > 5 μm counts to the same extent as dry ice. Thus, temperature-dependent shifts in particle size distribution consistent with aerosol swelling were observed and were maximised at -78.5°C, when dry ice was used as a coolant.

We next evaluated the performance of 3D-printed PBM-Hale™ prototype under tidal breathing and dry ice (−78.5°C) condensation to determine sampling reproducibility and risk of salivary contamination (Fig. 2A-D). EBC specimen volumes increased linearly with sampling time for up to 30 mins of use by a single donor (Fig. 2A), demonstrating consistent capture of fine aerosols across different collection times ($r^2 = 0.9995$; average tidal EBC (TiEBC) sampling rate of 138.6 ± 13.7 µL/min). Next, we sought to determine whether labile biomarker levels were affected by the duration of sampling. 18S rRNA is present in all human biofluids and highly sensitive to degradation. RT-qPCR showed significant enrichment after 2 minutes of collection (4.761 ± 0.54-fold relative to background), increasing to 30.51 ± 0.14-fold after 10 minutes (Supplementary Fig. 2A). Total 18S rRNA yield increased proportionally with sampling duration (2–10 min, $r^2 = 0.9677$), mirroring the linear increase in EBC volume. Strong reproducibility was also evidenced by low inter-sample variability across five independent 2-minute collections from the same donor (Ct 28.34 ± 0.25; Supplementary Fig. 2B). Salivary alpha-amylase activity, a recognized biomarker of saliva contamination in EBC, was readily detected in drooled saliva and in LD fractions recovered from the separator saliva trap. In contrast, no activity was detectable in FA EBC (Fig. 2B), indicating efficient separation of saliva-containing LD from FA EBC.

EBC is estimated to suffer > 10,000x dilution of epithelial lining fluid [42]. Compared to sampling at ambient temperature (25°C) for 30min, dry ice condensation increased EBC specimen volume by ~ 13.9x (from 0.315 ± 0.006 mL to 4.383 ± 0.123 mL; Fig. 2C). Yet total protein concentration was reduced only by 2.2x (from 9.58 ± 0.44 µg/mL to 4.36 ± 0.67 µg/mL; Fig. 2D). The unexpectedly 6.32 ± 0.86 fold higher total protein mass recovered by dry ice condensation indicated improved capture of aerosolized particles in exhaled air, rather than simple gas-phase water dilution of aerosol solutes during condensation.

To better understand the sampling process, we used computational fluid and thermal dynamics modelling of typical 0.5 L, 5 second tidal breath duty cycles (Fig. 2E-F; Video 1). Flow path analysis showed turbulence in the separator during exhalation (0–3 seconds, Fig. 2F), supporting experimental findings of efficient saliva droplet elimination. Furthermore, the first 416 mL of the 500 mL tidal exhalation column flowed through the specimen vial, interestingly with no appreciable temperature drop in the bulk flow phase, even under dry ice condensation. During inhalation (4–5 seconds), however, the separator one-way valve prevented inhalation flow via the device, leaving 48 mL of end-tidal exhaled breath stationary in the specimen vessel. These 2 seconds were sufficient to maximally cool all the end-tidal exhaled air remaining in the vessel (Fig. 2F). Computational modelling therefore corroborated particle counting data to suggest that EBC sampling with PBM-Hale™ under dry ice condensation was focused on distal airway aerosols present in the last 48mL of each exhalation.

To confirm the origin of dry ice-condensed PBM-Hale™ specimens, we next measured levels of SP-D, which is enriched in alveolar fluid. Additionally, the concentrations of a panel of inflammatory biomarkers were determined using the Meso Scale Discovery V-PLEX platform. EBC sampling of healthy participants was performed using two breathing manoeuvres: tidal breathing (TiEBC) and singing (SiEBC). Across the 14-plex inflammatory marker panel, 80% of TiEBC and SiEBC samples were above the lower limit of quantification (LLQ) for 9/14 and 8/14 tested markers, respectively (Fig. 2G; Sup. Figure 3). For TiEBC, interleukin (IL) 1β, IL-2, IL-6, IL-8, IL-10, IL12p70, IL-13, interferon (IFN)-γ, and tumor necrosis factor (TNF)-α were quantifiable in at least 80% of TiEBC samples. Similar patterns were observed for SiEBC, with only TNF-α falling below this threshold. IL-4, IL-5 and granulocyte/macrophage colony stimulating factor (GM-CSF) were quantifiable in

both TiEBC and SiEBC, albeit in a lower proportion of samples, while IL-17A and IL-12/IL-23p40 were not quantifiable in either sampling modes. Among inflammatory markers quantifiable in > 80% of samples, concentrations in neat EBC were in the low pg/mL range, spanning from 0.43 ± 0.54 pg/mL and 0.22 ± 0.13 pg/mL (IL-10) to 1.65 ± 0.57 and 1.35 ± 0.22 pg/mL (IFN-γ) in TiEBC and SiEBC, respectively (Supplementary Fig. 3). SP-D concentrations (Fig. 2I), however, were substantially higher at 72.62 ± 85.09 and 104.8 ± 93.90 pg/mL in TiEBC and SiEBC, respectively. No differences in inflammatory mediator or SP-D concentrations were observed between the two breathing manoeuvres, an expected finding as singing is not known to induce lower respiratory tract inflammation. The relative enrichment of SP-D, irrespective of exhalation manoeuvre, corroborated thermodynamic modelling and further supported preferential condensation of lower respiratory tract aerosols.

Together with the absence of salivary alpha amylase activity, these data demonstrated that the novel PBM-Hale™ EBC collector, when operated with dry ice as a coolant, reproducibly sampled saliva-free EBC enriched for distal airway biomarkers, without affecting their stability.

Supplementary Fig. 1. Aerosol particles count at the PBM-Hale™ exhaust during 3 minutes of tidal breathing (n = 3/group), with condensation temperature (Tcond) at -78.5 ^{o}C (dry ice), 0 ^{o}C (wet ice) or 25 ^{o}C (room temperature) showing temperature-dependent depletion of ultrafine particles (< 0.3 µm) and enrichment of larger particle sizes. Increased counts (counts per second; cps) of 0.5–10 µm particles (dry ice) and 1–5 µm particles (wet ice) consistent with aerosol swelling and enhanced capture at lower temperatures (optimum with dry ice). Counts presented in interval bins of (A) < 0.3 µm, (B) 0.3–0.5 µm, (C) 0.5-1 µm, (S) 1.0-2.5 µm, (E) 2.5-5 µm, and (F) 5–10 µm, with violin plots showing medians and quartiles; *p < 0.05; **p < 0.01; ***p < 0.001; ****p < 0.0001; ns: not significant.

Supplementary Fig. 2. Reproducible and collection-time dependent detection of 18S rRNA in PBM-Hale™ breath condensates. 18S rRNA levels were determined by pan-eukaryotic Taqman® assay in extracted RNA from FA EBC samples captured at -78.5 ^{o}C from an adult male healthy volunteer for (A) 2-10 minutes vial tidal breathing or (B) over 2 minutes, 5 independent times. Each point in the graph represents the mean of duplicate RT-PCR technical replicates. In (B), Ct values for a nasal swab sample obtained from an adult healthy male volunteer and RNase free water were used as positive and negative control, respectively.

Supplementary Fig. 3. I**nflammatory markers in PBM-Hale™ breath condensates collected using dry ice.** Inflammatory markers were quantified in the distal FA collected via tidal breathing (TiEBC) or singing (SiEBC) for 15 and 30 minutes, respectively; n = 10 healthy volunteers. A 14-plex panel (Mesoscale Discovery V-plex) was used to determine levels of each marker. Dashed red lines represent the LLQ each marker. TiEBC *vs* SEBC *: p < 0.05, statistically different as analysed by paired T test. All other markers are not significantly different by paired t test or Wilcoxon matched-pairs signed rank test.

PBM-Hale™ captures viruses and nanoparticles suspended in fine aerosols

To ascertain the utility of PBM-Hale™ specimens for detecting LRTIs, we first tested the impact of nebulisation and PBM-Hale™ condensation on virus infectivity. Using a GFP-expressing lentivirus, pseudotyped with VSV glycoprotein (VSV-GFP), mechanically nebulised virions were passively diffused

through PBM-Hale™ (Fig. 3A). Condensates were then incubated with HEK293T cells and GFP expression was assessed by flow cytometry and fluorescence microscopy (Fig. 3B-C) after confirming pseudotyped virus stability to 1:14 dilution with deioinsed water, and extended room temperature incubation (Supplementary Fig. 4). Nebulised virion infectivity was reduced due to nebulisation and as a function of condensation temperature by 33% (0°C) and 66% (-78.5°C) versus control virion suspensions (Fig. 3B-C). These experiments suggested that PBM-Hale™ could sample infectious virions suspended in FA EBC.

To better understand how nebulization, condensation, and particle charge interact in affecting nanoparticle structural integrity, we repeated the nebulisation experiments using PS beads (-71mV, 118nm), negatively charged liposomes (-72 mV, 188nm), neutral liposomes (-20 mV, 168nm), lentiviral VLPs (VLP-L; -31 mV, 193nm) and SARS-CoV-2 VLPs (-17mV, 155nm). We measured the resulting changes in particle size and concentration after nebulization and condensation with PBM-Hale™ using NTA. Changes were compared to control samples, and samples subjected to a -78.5 ^{o}C freeze-thaw cycle (Fig. 3D-E, Sup. Figure 5). In line with the VSV-GFP infectivity assay, VLP-L concentration was reduced by 43.7% with a corresponding reduction in particle diameter of 29.4% on account of nebulization/condensation ($p < 0.0001$), but not by freezing of the suspension (2.8% reduced concentration, 1.3% reduction in mean size, n = 3). Interestingly, no appreciable change in SARS-CoV-2 VLP particle concentration ($p > 0.999$) was observed suggesting that PBM-Hale™ capture of SARS-CoV-2 could potentially have minimal impact on virion integrity. It must be noted that SARS-CoV-2-VLPs, unlike lentiviral VLPs, were not fluorescently tagged and tracked by scatter-NTA instead of fluorescence-NTA and non-VLP particles may thus be included in this analysis. By stark contrast, negatively charged nanoparticle concentration in PBM-Hale™-captured condensates was reduced by 72.6–98.0 times compared to source fluids ($p < 0.0001$), likely on account of freezing-driven aggregation, in a nanoparticle type-dependent manner; PS beads ($p < 0.0001$) > liposomes ($p = 0.0031$). Taken together, these results supported the evaluation of tidal breath SARS-CoV-2 emission using PBM-Hale™.

Supplementary Fig. 4. Viral solution dilution (reflecting condensation-driven dilution of breath condensate specimens) does not affect viral infectivity. (A-B) Two pseudotyped lentiviruses, a GFP-reporter D614G SARS-CoV-2 spike-pseudotyped lentivirus (A) or rabies glycoprotein-pseudotyped lentivirus (B) were incubated for 0, 30, or 60min after 1:14 dilution in 18 megaOhm water, and were subsequently seeded onto HEK293T cells for 72h to assess impact on infectivity. (C) GFP-reporter Beta variant SARS-CoV-2 spike-pseudotyped lentivirus was incubated at room temperature for 24h and impact on HEK293T cell infectivity was compared to 4 ^{o}C storage. Virus titres were calculated as the mean relative light units/min (n = 3, average ± standard deviation; data representative of 3 independent experiments.

Supplementary Fig. 5. Impact of condensation temperature on mechanically nebulized infectious pseudoviruses and synthetic nanoparticles. (A) A clinical grade nebulizer (PARI) was attached to PBM-Hale™ using a 3D printed adapter to passively route suspensions of nanoparticles into the condenser. (B) Titration of VSV-GFP lentivirus for the determination of 50% Tissue Culture Infectious Dose (TCID50) identifies a 2.5 log stock dilution as the appropriate concentration for the above-background detection of GFP positive cells by fCM (average ± standard deviation of 3 independent replicates). (C) Effect of flash-freezing or mechanical aerosolization/condensation capture of polysterene (PS) beads, liposomes, lentiviral virus-like particles, or SARS-CoV-2 virus-like particles on particle concentration as a function of particle diameter, as measured by

nanoparticle tracking analysis (average ± standard error of the mean of 3 independent replicates is depicted in the green-shaded area). The charge (zeta potential) of each particle type is shown.

Singing enhances viral and host RNA content without saliva contamination

The distal lung origin of bulk exhaled FA mass [3] motivated us early in the COVID-19 pandemic to ask whether tidally exhaled breath might be a source of airborne SARS-CoV-2. We therefore sampled COVID-19 patients by tidal oral exhalation using PBM-Hale™ cooled with dry ice for up to 30min and evaluated FA EBC fractions for SARS-CoV-2 by RT-PCR. The first 12 cases involved hospitalized patients either convalescent and nasopharyngeally negative for SARS-CoV-2 (n = 2; 3rd week from symptom onset), or within their first 5 days of hospitalization (n = 10; >2 weeks after symptom onset). All study participants were sampled in COVID-19 wards across 2 hospitals, with no high-efficiency particulate air (HEPA) filtration or mechanical ventilation of the ward rooms. Such settings were known to be heavily contaminated with airborne SARS-CoV-2 nucleic acid [43]. None of these samples returned any evidence of SARS-CoV-2 genomes in FA EBC, as the single sample with an inconclusive readout (Ct 38 in one of two assay targets) was negative on repeat testing. Given accruing evidence at the time of nasopharyngeal viral load and transmission declining within the first 5 days of symptom onset [44], we next recruited 30 acutely symptomatic patients (Supplementary Table 1) confirmed NPS-positive for SARS-CoV-2. No SARS-CoV-2 nucleic acid was detected among these 1.18mL ± 0.32 tidal FA EBC samples either, despite nasopharyngeal loads as low as Ct 13.1.

Separate studies [33, 45] suggested SARS-CoV-2 load may increase in exhalations as a function of vocalization intensity. We thus evaluated changes in PBM-Hale™ FA EBC viral load in a small cohort of acute cases in Brazil (Table 1; Fig. 4), as a function of tidal breathing *vs* singing (Fig. 5A). Patients were recruited among attendees of a suburban resource-limited primary care centre, and sampling was conducted in a highly naturally ventilated screening room.

Table 1
Participant characteristics in the tidal *versus* forced expiration FA EBC SARS-CoV-2 viral load study conducted in Brazil.

Characteristics	**Total n = 30**
Age, years (median, IQR)	42.5 (36.5–53.25)
Age groups, years (n, %)	
< 18	0 (0%)
18–69	30 (100%)
70–80	0 (0%)
Sex (n, %)	
Male	6 (27%)
Female	24 (73%)
Height (cm, ± SD)	164.10 ± 6.10
Weight (kg, ± SD)	76.66 ± 17.35
BMI	28.42 ± 5.92
< 18.5	0 (0%)
18.5–24.9	8 (27%)
25–29.9	12 (40%)
> 30	10 (33%)
Armspan (cm, ± SD)	160.3 ± 12.82
Days after symptom onset (n, ± SD)	3.93 ± 1.05
Symptoms (n, %)	
Fatigue	10 (33%)
Dyspnoea	0 (0%)
Diarrhoea	7 (23%)
Cough	24 (80%)
Rhinorrhoea	26 (87%)
Headache	20 (67%)
Muscle pain	14 (47%)
Joint pain	3 (10%)
Dysgeusia/Ageusia	3 (10%)

Characteristics	Total n = 30
Dysosmia/Anosmia	3 (10%)
Fever (> 37.5 ^{o}C; N, %)	0 (0%)
Other lung disease	
Asthma (n, %)	1 (7%)
Chronic bronchitis (n, %)	1 (7%)
Emphysema (n, %)	1 (7%)
COPD (n, %)	1 (7%)
Tuberculosis (n, %)	0 (0%)
Lung cancer (n, %)	0 (0%)
Lung fibrosis (n, %)	1 (3%)
Comorbidities (n, %)	8 (27%)
Lung Surgery (n, %)	0 (0%)

First, we evaluated if PBM-Hale™ sampling by singing impacts specimen yield, purity, and the levels of the specimen integrity biomarker 18S rRNA. FA EBC yield rates did not differ by exhalation mode (117.4 ± 44.59 µL/min *vs* 100.5 ± 48.57 µL/min; p = 0.2946; Fig. 5B), a finding attributable to the terminal 48mL of each breath being effectively condensed by PBM-Hale™ (Fig. 2). More importantly, singing did not compromise PBM-Hale™ FA EBC specimen purity, as only paired drooled saliva exhibited α-amylase activity. All TiEBC and SiEBC FA samples were free of detectable salivary contamination (Fig. 5C).

Despite sampling yields being similar between exhalation maneuvers, only SiEBC yield demonstrated correlations with physiological variables, such as body mass index (BMI; r = 0.517; p = 0.0048), arm span (r = 0.641; p = 0.0002), and age (years) x BMI (r = 0.429; p = 0.0227; Figs. 5D–G). SiEBC yield was also higher in overweight and obese patients (Fig. 5H). In contrast, self-reported symptoms such as fatigue and cough did not influence SiEBC mass (Figs. 5I–J), indicating that symptoms associated with COVID-19 do not impact specimen yield rates. Notably, cough episodes or interruptions during sampling did not correlate with EBC yield, indicating that coughing or brief pauses do not adversely affect EBC sampling (Fig. 5D).

Tidal FA EBC 18S rRNA results corroborated earlier findings (Supplementary Fig. 2) with levels averaging ~ 5 cycles above background (Ct 34.3 ± 1.5). In contrast, singing increased 18S rRNA content by approximately 90.6-fold (Ct 27.8 ± 1.90); in the absence of salivary α-amylase activity (Fig. 5C) these results suggested enrichment with distal airway contents (Fig. 5K) due to increased small airway fine aerosol generation [33, 45] and not of oral fluid nebulization [46]. Accordingly, SiEBC, but not TiEBC, yield rates correlated positively with 18S rRNA levels (Fig. 5L-M). These findings suggested that singing promoted distal airway FA EBC capture without salivary contamination, or compromising sampling feasibility in symptomatic patients.

Pulmonary SARS-CoV-2 RNA loads are higher than salivary loads and distinct to nasopharyngeal loads early after symptom onset

We next evaluated TiEBC and SiEBC samples alongside matched NPS, drooled saliva, and LD fractions recovered from the PBM-Hale™ separator, for the presence of SARS-CoV-2 RNA (Fig. 6). Of 30 confirmed COVID-19 participants, 24 with valid RT-PCR results were included in the final analysis after exclusion of two insufficient SiEBC samples, and four samples that failed RT-PCR negative controls on account of contamination on extraction documented by 18S rRNA in negative controls (Fig. 4).

Consistent with the observed enrichment of 18S rRNA during singing (Fig. 5), SARS-CoV-2 was detected in all SiEBC samples (24/24, 100%) and in 21/24 (87.5%) TiEBC samples, using a Poisson sensitivity detection criterion [47] (≥ 1/3 technical replicates Ct < 40 for N1 or N2; Table 2; Supplementary Table 2; Figs. 6B,C). Sensitivity analysis *vs* sampling time indicated 2min samples would have sufficed to achieve this outcome. Application of positive/inconclusive/negative RT-PCR outcome criteria [34] (i.e. positivity requiring Ct < 40 for N1 and N2 across all technical replicates), SiEBC yielded 17/24 (70.8%) SARS-CoV-2 positive detections, the remainder 7/24 (29.2%) classified as inconclusive. In the context of symptomatic disease, however, inconclusive results would classify these seven patients as likely SARS-CoV-2 positive. In contrast, none of the TiEBC samples met such stringent positivity criteria, with 21/24 (87.5%) classified as inconclusive and 3/24 (12.5%) as negative (not detected). Unlike siEBC samples, which yielded SARS-CoV-2 RT-PCR Ct values as low as 25.42, only one TiEBC sample, classified as inconclusive, was detectable above the assay limit of quantification (Ct = 34.3). Interestingly, detection rates in SiEBC substantially exceeded those in paired LD fractions isolated from the separator saliva trap (29.2% positive, 70.8% inconclusive SiLD samples *versus* 70.8% positive, 29.2% inconclusive SiEBC samples; Table 2), arguing against saliva-derived carryover as the primary source of viral RNA in SiEBC.

Table 2

Summary of SARS-CoV-2 (2019-nCov RT-PCR diagnostic panel) and host 18S RT-PCR data generated by testing NP swab, saliva and EBC obtained via tidal and singing maneuvers.

Specimen type	**SARS-Cov-2 (n = 24 participants)**					**Ct[1, 3] mean ± SD**		**ΔCt[3] mean ± SD**
	Poisson sensitivity criteria [35, 86]		**Positive/inconclusive/negative RT-PCR outcome criteria [34]**					
Positive ≥ 1/3 replicates Ct < 40 for N1 or N2	**Negative 0/3 replicates Ct < 40 for N1 and N2**	**Positive 3/3 replicates Ct < 40 for N1 and N2**	**Inconclusive 1–2 out of 3 replicates Ct < 40 for N1 and/or N2**	**Negative 0/3 replicates Ct < 40 for N1 and N2**	**N1/N2**	**18S[4]**		
NPS[2]	24/24 (100.0%)	0/24 (0.0%)	24/24 (100.0%)	0/24 (0.0%)	0/24 (0.0%)	24.25 ± 3.81 n = 24	21.87 ± 2.64 n = 24	2.38 ± 3.49 n = 24
Saliva	23/24 (94.8%)	1/24 (5.2%)	22/24 (91.7%)	1/24 (4.17%)	1/24 (5.2%)	26.86 ± 3.89 n = 22	19.56 ± 1.45 n = 22	7.30 ± 3.64 n = 22
Tidal EBC	21/24 (87.5%)	3/24 (12.5%)	0/24 (0.0%)	21/24 (87.5%)	3/24 (12.5%)	-[5]	34.10 ± 1.40 n = 23	-
Singing EBC	24/24 (100.0%)	0/24 (0.0%)	17/24 (70.8%)	7/24 (29.2%)	0/24 (0.0%)	30.54 ± 3.12 n = 17	27.38 ± 1.69 n = 17	3.16 ± 2.73 n = 17
Tidal large droplets	15/24 (62.5%)	9/24 (37.5%)	2/24 (8.3%)	13/24 (54.2%)	9/24 (37.5%)	33.08 ± 2.43 n = 2	28.16 ± 9.93 n = 2	4.92 ± 7.49 n = 2
Singing large droplets	24/24 (100.0%)	0/24 (0.0%)	7/24 (29.2%)	17/24 (70.8%)	0/24 (0.0%)	32.37 ± 1.63 n = 7	28.99 ± 1.71 n = 7	3.38 ± 1.63 n = 7

1. Ct: cycle threshold; 2. NPS: nasopharyngeal swab. 3. Mean Ct and ΔCt values (final three columns) are shown only for samples positive for SARS-CoV-2 according to the positive/inconclusive/negative RT-PCR outcome criteria (3/3 replicates with Ct < 40 for both N1 and N2). 4. 18S Ct values are shown only for specimens positive for SARS-CoV-2 according to the positive/inconclusive/negative RT-PCR outcome criteria (except for TiEBC, where no specimen achieved this SARS-Cov-2 positivity criteria). 5. No N1/N2 or ΔCt data are shown for TiEBC, as none of the 24 samples were positive for SARS-CoV-2 by the positive/inconclusive/negative RT-PCR outcome criteria. TiEBC = Exhaled breath condensate collected via tidal breathing. SiEBC = Exhaled breath condensate collected via a singing maneuver.

Supplementary Table 1. Participant characteristics in the tidal FA EBC SARS-CoV-2 viral load study conducted in Greece.

Spectrophotometry on RNA extracts produced with automated or column-based methods did not yield quantifiable results. Given the robustness of 18S rRNA as an endogenous RNA integrity marker for eukaryotic specimens, we next compared normalized (ΔCt) SARS-CoV-2 RNA levels amongst matched specimen types (Fig. 6H-M). Normalized SARS-CoV-2 RNA levels in SiEBC correlated with viral RNA levels in saliva ($r = 0.7412$, $p = 0.0015$) and LD fractions ($r = 0.8929$, $p = 0.0123$), but not with NP swab RNA levels ($r = 0.2990$, $p = 0.2430$); Fig. 6I-K. Interestingly, normalized SiEBC viral loads were lower than those of paired NP swabs, but higher than those in saliva (Fig. 6G–M). Together with the lower positivity rate in LD fractions and the absence of salivary α-amylase in FA EBC, these findings favoured a pulmonary instead of salivary origin of SARS-CoV-2 RNA in singing-derived end-tidal EBC captured with PBM-Hale™. Although a positive correlation between age and normalised viral RNA load was identified in these participants (Fig. 7), none required hospitalisation or had negative outcomes on follow-up up to 87 days after recruitment.

Exploratory multiplex cytokine profiling by Luminex demonstrated limited sensitivity in EBC, with ≤ 40% of TiEBC and ≤ 20% of SiEBC specimens above the lower limit of quantification for most analytes (Supplementary Fig. 6). This contrasted markedly with observations among healthy subjects (Fig. 2; Supplementary Fig. 3), but reflected the higher manufacturer-reported sensitivity of Meso Scale Discovery *vs* Luminex assays in serum samples. Nevertheless, elevated IL-4 levels (> 15 pg/mL) were detected in 6/15 SiEBC samples. The results represent potentially two orders of magnitude higher concentrations in the patient cohort *vs* healthy participant data, warranting further investigations of pulmonary inflammation with PBM-Hale™ in the future.

Collectively, our findings confirm that singing enhances total RNA content (Fig. 5K) in addition to viral RNA in exhaled aerosols [45], even in end-tidal fine aerosol fractions. Moreover, effective saliva droplet contamination prevention, can non-invasively deliver clinically meaningful pulmonary data independent to the oral and upper airway compartments.

Supplementary Fig. 6. Inflammatory markers in small airway breath condensates from COVID-19 patients. COVID-19 NPS positive patients (n = 15) provided FA EBC by tidal breathing for 30 minutes (TiEBC) or by singing “Happy birthday” in Portuguese for 15 minutes (SiEBC) into the PBM-Hale™ prototype. The coolant chamber was loaded with dry ice to provide − 78.5°C fine aerosol condensation. A 14-marker panel (MILLIPLEX® MAP human cytokine / chemokine magnetic bead panel 96 well plate assay) was used and levels of each marker in TiEBC and SiEBC are shown in pg/mL. Dashed red lines represent the LLQ of the immunoassay. TiEBC *vs* SEBC *: $p < 0.05$, statistically different as analysed by paired T test. All other markers are non-significantly different by paired t test or Wilcoxon matched-pairs signed rank test.

DISCUSSION

The key problems of sampling inconsistency, salivary contamination, and sample loss among EBC collectors [3, 20] gave rise to criticisms [48] over EBC biomarker associations with disease. These challenges persist, restricting clinical translation of this methodology [49, 50]. Many problems relate to the architecture of EBC collectors. For example, unprotected sampling surfaces (petri dishes, filters, mask strips, or open-ended condensing tubes) risk ambient aerosol condensation and manual handling contamination. Elephant trunk ventilator connectors suffer aerosol ‘rain out’ prior to sampling. Nevertheless, high natural variability in

exhaled aerosol particle load [51] and exhaled breath relative humidity as low as 30% [52] may contribute to inconsistent observations. Conversely, some devices lack physical means of salivary droplet separation, resulting in substantial saliva contamination [53, 54]. Importantly, this risk can be missed if poorly sensitive analytical methods are used [55]. Yet other devices [56–58], can easily suffer saliva droplet contamination in conducting tubing. 'Fluid film burst' [1] disruption of saliva droplets may generate contaminating salivary FA, in some cases propelling large droplets into the condenser, especially if tubing is angled downwards [56, 59].

We sought to address EBC sampling inconsistency, salivary contamination, and sample loss by a) preventing sample loss in non-condensing instrument parts; b) physically isolating the condensing surface to prevent environmental contamination or evaporative sample loss; and c) implementing basic principles from inhaled therapeutics design [60] to separate saliva-laden LD from the FA. Our approach avoided defined or average pore sizes prone to wetted-filter nebulization, to deliver reliable sampling yield rates (Fig. 2); small changes in device architecture proved critical in preventing loss of linearity or saliva contamination. Similar observations have also been reported by diverting exhaled breath flow to reduce salivary contamination [54]. In our case however, any contaminating saliva in the FA fraction was below salivary α-amylase assay detection limits, corresponding to a matched saliva dilution, if any, of > 1,750-fold.

Condensate dilution is unavoidable and underpins 500x sample concentration recommendations to detect analytes reliably [53]. However, we observed only ~ 14x dilution since PBM-Hale™ drives exhaled particle enlargement and protein capture increase by ~6x. This phenomenon is likely universal among devices where breath remains static in the condenser during inhalation. Condensation temperature decay in some systems will reduce exhaled particle swelling and thermophoresis as condenser temperature rises, explaining well-established sampling and specimen biomarker inconsistencies [3]. Insulated dry ice cooling can sustain reliable EBC capture for 30 min of continuous use. Moreover, the resulting specimens return consistent inter-specimen, and healthy participant data even when highly labile biomarker levels are assessed. Relatively high levels of lung surfactant protein, in the absence of salivary amylase contamination, and in the context of preferential condensation of end-expiration fine aerosols, thus point to PBM-Hale™ efficiently sampling aerosols derived from lower respiratory tract epithelial lining fluid.

Airborne SARS-CoV-2 transmission [4, 61, 62], often held responsible for superspreading [63–66] against ~ 30% false negative error rates of NPS RT-PCR [67, 68], has motivated research on breath aerosols as a source of infection. Outcomes have ranged 0% [59] to 93% [69] of cases NPS-positive for SARS-CoV-2 also yielding breath samples positive for the virus. Studies involved devices previously reported [69] or readily prone [57–59, 70] to salivary contamination, an established source of SARS-CoV-2 [71], with important exceptions. In Feng *et al.*, a 35L breath-and-air mixing container was connected on its upper surface to a pump. Aerosols were pumped into a NIOSH bioaerosol collector, inertially/gravitationally excluding LDs: air-diluted tidal breath samples were devoid of SARS-CoV-2 RNA. However, in Huang *et al.*, 'classical' EBC collected using a 15mL tube with its cut-off tip conducting to a 50 mL receptacle immersed in coolant, lacking any environmental or salivary contamination prevention, was positive in 25% of cases. In the latter study, negative breath samples were also matched by salivary negative samples in patients positive by NPS, pointing to saliva as the source of 'breath' SARS-CoV-2. Elsewhere, electret filter-based testing did return high concordance in exhaled breath viral load *vs* nasopharyngeal swabs [72]. Yet this technology does not prevent large droplet contamination of

the breath filter and has only been explicitly tested for methadone capture efficiency, as opposed to particle size filtering [72, 73].

A salivary source cannot be excluded either from the seminal reports of Coleman *et al.* [33] and Adenaiye et al. [33] that established airborne transmission as a material risk. Infectious SARS-CoV-2-laden exhalations were detected in tidal breath, rising in concentration by vocalization intensity. The studies evacuated patient exhalations at a 130L/min fixed rate through a ~1m long cone surrounding the patient's head, and into an aerosol capture array with a 5 μm pore partition [74]. Humidified air supply at the cone perimeters in Coleman *et al.* was ambient, 68% relative humidity HEPA-filtered air in a COVID-19 ward (Coleman K, personal communication). This reduced the likelihood of ambient contamination, but retained fomite risks from participant hair or skin. Moreover, the device did not dynamically adjust suction rate in response to patient exhalation patterns e.g. during singing vs tidal breathing. This could result in flow changes at the cone perimeter, exacerbating fomite risks. Moreover, sharp temperature and humidity gradients from the respiratory tract to the cone atmosphere would change aerosol particle size distribution. Vacuum pressure drop, cone path length, ambient air influx, and mixing within the cone would exacerbate this effect [75]. In their equally seminal paper on this sampling method, McDevitt *et al.* [74] reported no ambient air FA particle size changes on account of the device cone and pump operation, but < 50% capture efficiency for mechanical aerosol particles < 30μm; no particle data was reported for human breath aerosols which differ in humidity and temperature to environmental aerosols.

Similar sampler design studies who found SARS-CoV-2 mainly in FA, also call for research in non-hospitalised cases [76]. Our study addresses this gap and corroborates predicate findings [45] on singing increasing viral RNA emission. We additionally find that singing also increases condensate 18S rRNA levels by ~ 91-fold, but Rnase P levels remain undetectable. Further research is warranted on the source and nature of the non-viral RNA-content in saliva-free EBC. It is notable that our sensitivity analysis indicated a 2 min singing specimen captured with our device, of which 20% is subjected to RT-PCR, would suffice for SARS-CoV-2 RNA detection among all participants, on viral Ct levels alone. By normalizing viral RNA loads for 18S rRNA levels, however, we additionally show that singing aerosols have 85-fold higher viral RNA concentrations compared to paired saliva samples, and are not associated to NPS fluid, excluding both mucosal sites as contamination sources. Together with the absence of α-amylase in the aerosol fraction, these findings point away from oral or vocal chord fluid aspiration/aerosolisation during singing, and towards a distinctly lower respiratory tract source.

Study limitations

Our findings are limited by the lack of SARS-CoV-2 infectious load determination in LD and FA fractions; residual (~ 0.01mL or < 10 sec breath) specimens proved insufficient for plaque forming assays. Participant numbers for this observational study were adequate for a specimen agreement pilot *versus* saliva and NPS, but the design could not address specificity and negative percent agreement. Larger studies are necessary to determine specimen utility in lower respiratory tract infection detection. In addition, specimen collection in Greece and Brazil was carried across two SARS-CoV-2 variant waves; differences in virus epithelium tropism early on disease onset have not been reported but cannot be excluded.

Particle emission rates rise and particle size distribution changes with increased volume of speech as well as coughing, and could be phoneme-derived [77–80]. These effects were not accounted for herein, nor were 18S rRNA level changes in singing COVID-19 patients corroborated with healthy participants. However coughing droplets did not affect aerosol yield rates, result in saliva contamination, or associate with higher 18S or rRNA viral loads. The study also did not randomize singing and tidal sampling. RNA biomarker correlations in tidal breathing specimens were not robust due to low detectability: protracted sampling protocols (> 30min) and significant specimen pre-concentration may therefore be required for studying analytes in tidally collected, saliva-free EBC.

Reliable use of immunoassays requires optimisations for each sample matrix, which was not attempted in this study. As with most BAL research, we instead used manufacturer-recommended protocols for human serum, to note consistent detectability and concentrations with independent reports for healthy participant BAL fluid [81–83]. Unlike 18S rRNA no endogenous normalization factor was used for cytokine and SP-D levels; yet protein biomarker concentrations did not comparably increase during singing. Total protein, albumin, or urea levels [84, 85], could also be relevant in future studies with PBM-Hale™. These would require high sensitivity assays as previously recommended for EBC investigations [3].

Conclusions

We have evaluated the performance of a novel EBC collector design that sought to overcome the key challenges of salivary/ambient contamination, sampling inconsistency and biomarker variability [3, 20]. This was achieved in a hand-held format by implementing turbulent inertial droplet impaction ahead of end-expiration FA condensation in a high thermal capacity condenser. Highly consistent lower respiratory aerosol condensates were collected by stationary vapour nucleation in the specimen vial during the inspiration phase of the breath cycle, promoting highly charged particle aggregation and enlarging aerosols to increase capture efficiency by 6x. The resulting lower respiratory EBCs have less than 1:1,750 contamination of saliva, are enriched for SP-D, and very low levels of cytokines in healthy participants. Use in poorly ventilated clinical wards confirmed absence of collector contamination with SARS-CoV-2 RNA by molecular testing, whilst efficient SARS-CoV-2 RNA detection, required singing for as little as 2 min. The study corroborates previous aerosol reports, with 18S rRNA normalization evidencing higher viral RNA loads in the lung, at least in the first 5 days from COVID-19 symptom onset. These results support further evaluation of this novel EBC collector in the diagnosis and management of respiratory diseases in the future.

Abbreviations

ELF
epithelial lining fluid
LRTI
lower respiratory tract infection
EBC
exhaled breath condensate
rRNA
ribosomal RNA

SP-D
surfactant protein D
FA
fine aerosols
LD
large droplets
BAL
bronchoalveolar lavage
ELISA
enzyme-linked immunosorbent assay
RT-PCR
reverse transcription polymerase chain reaction
VOC
volatile organic compounds
NPS
nasopharyngeal swab
Ct
threshold cycle
GFP
green fluorescent protein
VSV
vescicular stomatitis virus
RABV
rabies virus
DOPC
dioleoylphosphatidylcholine
DOPS
dioleoylphosphatidylserine
PC
phosphatidylcholine
VLP
virus-like particles
TiEBC
Tidal breathing-produced EBC
SiEBC
Singing-produced EBC
LLQ
lower limit of quantification
IL
interleukin
TNF
tumor necrosis factor

GM-CSF
granulocyte/macrophage colony stimulating factor
VLP-L
lentiviral VLPs
HEPA
high-efficiency particulate air

Declarations

Ethics Approval and Consent to Participate:

All healthy volunteer EBC samples were obtained with participant informed consent under Northumbria University ethics application no. 43341 approved by the Department of Applied Sciences Subcommittee of the University Research Ethics Committee. All COVID-19 patient EBC samples were collected with informed consent under the National and Kapodistrian University of Athens General Hospital 'Evangelismos' ethics application protocol no. 280/24-4-2020 approved by the Scientific Committee of the General Hospital 'Evangelismos' and approval no. 54358021.1.0000.5149 by the Institutional Review Board of the Federal University of Minas Gerais.

Competing Interests

Prof. Moschos and Prof. I. Kale co-invented PBM-Hale™ (patent no. WO2017153755). Prof. Moschos, Prof. Kale, Dr. Torgul, and Northumbria University are shareholders to the Northumbria University spinout company PulmoBioMed Ltd. Prof. S. A. Moschos, Dr. M. A. Sugimoto, and Mr. S. Ali are employees of PulmoBIoMed Ltd. All other authors declare no competing interests.

Funding:

This project was supported by the InnovateUK iCURE III project no. 43055, and the Northern Accelerator II project no. 25R18P02557. JAM received funding from the German Research Foundation. Airborne particle size analysis was enabled by the kind loan of equipment by Particles Plus Inc.

Author Contribution

SAM conceived and designed in collaboration with IK the new EBC collector, printing early prototypes with the assistance of VT. SA, MC, and SAM performed the production-scale computer aided design and production work and, with the assistance of PH, the computational flow modelling. JH, RG, JAM, TM, SA, EW, LU, BA, and AW performed all the experimental laboratory work under the supervision and direction of JM, AN, and SAM who designed the experimental work and participated in the data analysis and interpretation. The clinical studies were designed by SAM and executed by EJ, NA, PJA, and TN under the supervision of PK, DPK, AT, AK, and MMT. Clinical samples were analysed by AZ, CR, and DCQ under the supervision of GM, PL, RSA, and

MMT. MAS performed all clinical data correlations and interpretations. JH, MAS and SAM co-authored the manuscript.

Acknowledgement

We thank Professors Aris Katzourakis, Giorgios Sourvinos, and Sir Peter J Barnes FRS and Manfred Frick regarding study societal impact considerations, organisational aspects of conducting sampling at PAGNI Hospital, and with manuscript review, respectively.

Data Availability

The datasets supporting the conclusions of this article are included within the article and its additional files

References

1. Johnson GR, Morawska L. The mechanism of breath aerosol formation. J Aerosol Med Pulm Drug Deliv. 2009;22(3):229–37.
2. Duguid JP. The size and the duration of air-carriage of respiratory droplets and droplet-nuclei. J Hyg (Lond). 1946;44(6):471–9.
3. Horvath I et al. A European Respiratory Society technical standard: exhaled biomarkers in lung disease. Eur Respir J, 2017. 49(4).
4. Greenhalgh T, et al. Ten scientific reasons in support of airborne transmission of SARS-CoV-2. Lancet. 2021;397(10285):1603–5.
5. Noakes CJ, et al. Modelling the transmission of airborne infections in enclosed spaces. Epidemiol Infect. 2006;134(5):1082–91.
6. Bourouiba L. Turbulent Gas Clouds and Respiratory Pathogen Emissions: Potential Implications for Reducing Transmission of COVID-19. JAMA. 2020;323(18):1837–8.
7. Montuschi P, et al. Exhaled 8-isoprostane as an in vivo biomarker of lung oxidative stress in patients with COPD and healthy smokers. Am J Respir Crit Care Med. 2000;162(3 Pt 1):1175–7.
8. Montuschi P, Barnes PJ. Exhaled leukotrienes and prostaglandins in asthma. J Allergy Clin Immunol. 2002;109(4):615–20.
9. Wells K, et al. Exhaled breath condensate pH assays are not influenced by oral ammonia. Thorax. 2005;60(1):27–31.
10. Milton DK, et al. Influenza virus aerosols in human exhaled breath: particle size, culturability, and effect of surgical masks. PLoS Pathog. 2013;9(3):e1003205.
11. Hunt J. Exhaled breath condensate: An evolving tool for noninvasive evaluation of lung disease. J Allergy Clin Immunol. 2002;110(1):28–34.
12. Shi M, et al. Initial development and testing of an exhaled microRNA detection strategy for lung cancer case-control discrimination. Sci Rep. 2023;13(1):6620.

13. Rubio K, et al. Preliminary results from the EMoLung clinical study showing early lung cancer detection by the LC score. Discov Oncol. 2023;14(1):181.
14. Pierre-Louis Odoom J, et al. Exhaled breath condensate identifies metabolic dysregulation in patients with radiation-induced lung injury. Am J Physiol Lung Cell Mol Physiol. 2023;324(6):L863–9.
15. Paris D et al. *NMR Profiling of Exhaled Breath Condensate Defines Different Metabolic Phenotypes of Non-Cystic Fibrosis Bronchiectasis.* Int J Mol Sci, 2020. 21(22).
16. Kowal K, Gielicz A, Sanak M. The effect of allergen-induced bronchoconstriction on concentration of 5-oxo-ETE in exhaled breath condensate of house dust mite-allergic patients. Clin Exp Allergy. 2017;47(10):1253–62.
17. Zhang S, et al. Rapid Measurement of Lactate in the Exhaled Breath Condensate: Biosensor Optimization and In-Human Proof of Concept. ACS Sens. 2022;7(12):3809–16.
18. Bach JP, et al. Measuring Compounds in Exhaled Air to Detect Alzheimer's Disease and Parkinson's Disease. PLoS ONE. 2015;10(7):e0132227.
19. Riepl RL, et al. Accuracy of 13C-urea breath test in clinical use for diagnosis of Helicobacter pylori infection. Z Gastroenterol. 2000;38(1):13–9.
20. Horvath I, et al. Exhaled breath condensate: methodological recommendations and unresolved questions. Eur Respir J. 2005;26(3):523–48.
21. Watson A, Wilkinson TMA. Respiratory viral infections in the elderly. Ther Adv Respir Dis. 2021;15:1753466621995050.
22. Saglani S, Menzie-Gow AN. Approaches to Asthma Diagnosis in Children and Adults. Front Pead. 2019;7:148–148.
23. Atlas RM. Bioterrorism: From Threat to Reality. Annu Rev Microbiol. 2002;56(1):167–85.
24. Feinberg T, et al. Cancerous glucose metabolism in lung cancer-evidence from exhaled breath analysis. J Breath Res. 2016;10(2):026012.
25. Barash O, et al. Differentiation between genetic mutations of breast cancer by breath volatolomics. Oncotarget. 2015;6(42):44864–76.
26. Antoniou SX, et al. The potential of breath analysis to improve outcome for patients with lung cancer. J Breath Res. 2019;13(3):034002.
27. Tiele A et al. Breath Analysis Using eNose and Ion Mobility Technology to Diagnose Inflammatory Bowel Disease-A Pilot Study. Biosens (Basel), 2019. 9(2).
28. de Vries R et al. Clinical and inflammatory phenotyping by breathomics in chronic airway diseases irrespective of the diagnostic label. Eur Respir J, 2018. 51(1).
29. Motamedi-Fakhr S, et al. Reference equations for tidal breathing parameters using structured light plethysmography. ERJ Open Res. 2021;7(2):00050–2021.
30. Bou Jawde S, et al. Tracking respiratory mechanics around natural breathing rates via variable ventilation. Sci Rep. 2020;10(1):6722.
31. Sumarokov V, Stachowiak P, Jezowski A. Low-temperature thermal conductivity of solid carbon dioxide. Volume 29. Low Temperature Physics - LOW TEMP PHYS; 2003. pp. 449–50.

32. Maass O, Barnes WH, Barnes HT. *Some thermal constants of solid and liquid carbon dioxide.* Proceedings of the Royal Society of London. Series A, Containing Papers of a Mathematical and Physical Character, 1926. 111(757): pp. 224–244.
33. Coleman KK, et al. Viral Load of SARS-CoV-2 in Respiratory Aerosols Emitted by COVID-19 Patients while Breathing, Talking, and Singing. Clin Infect Dis; 2021.
34. Lu X, et al. Enhanced throughput of the severe acute respiratory syndrome coronavirus 2 (SARS-CoV-2) real-time RT-PCR panel by assay multiplexing and specimen pooling. J Virol Methods. 2021;293:114149.
35. Taylor SC, et al. The Ultimate qPCR Experiment: Producing Publication Quality, Reproducible Data the First Time. Trends Biotechnol. 2019;37(7):761–74.
36. Ruiz-Villalba A, Ruijter JM, van den Hoff MJB. Use and Misuse of Cq in qPCR Data Analysis and Reporting. Life (Basel), 2021. 11(6).
37. Shah K, et al. Field-deployable, quantitative, rapid identification of active Ebola virus infection in unprocessed blood. Chem Sci. 2017;8(11):7780–97.
38. Grigorov B, et al. Rapid titration of measles and other viruses: optimization with determination of replication cycle length. PLoS ONE. 2011;6(9):e24135.
39. Conzelmann C, et al. Salivary extracellular vesicles inhibit Zika virus but not SARS-CoV-2 infection. J Extracell Vesicles. 2020;9(1):1808281.
40. Schütz D, et al. Negatively Charged Peptide Nanofibrils from Immunoglobulin Light Chain Sequester Viral Particles but Lack Cell-Binding and Viral Transduction-Enhancing Properties. ACS Omega. 2021;6(11):7731–8.
41. Xu R et al. Construction of SARS-CoV-2 Virus-Like Particles by Mammalian Expression System. Front Bioeng Biotechnol, 2020. 8.
42. Davis MD, Montpetit AJ. Exhaled Breath Condensate: An Update. Immunol Allergy Clin North Am. 2018;38(4):667–78.
43. Ong SWX, et al. Air, Surface Environmental, and Personal Protective Equipment Contamination by Severe Acute Respiratory Syndrome Coronavirus 2 (SARS-CoV-2) From a Symptomatic Patient. JAMA. 2020;323(16):1610–2.
44. Tindale LC et al. *Transmission interval estimates suggest pre-symptomatic spread of COVID-19.* medRxiv, 2020: p. 2020.03.03.20029983.
45. Adenaiye OO, et al. Infectious SARS-CoV-2 in Exhaled Aerosols and Efficacy of Masks During Early Mild Infection. Clin Infect Dis; 2021.
46. Morawska L, et al. Size distribution and sites of origin of droplets expelled from the human respiratory tract during expiratory activities. J Aerosol Sci. 2009;40(3):256–69.
47. Patterson B, et al. Cough-independent production of viable Mycobacterium tuberculosis in bioaerosol. Tuberculosis (Edinb). 2021;126:102038.
48. Hyde RW. I don't know what you guys are measuring but you sure are measuring it! A fair criticism of measurements of exhaled condensates? Am J Respir Crit Care Med. 2002;165(5):561–2.
49. Garcia-Marcos L. Exhaled breath condensate in asthma: Are we stupid if we do not keep it simple? Allergol Immunopathol. 2017;45(1):1.

50. Popov TA, et al. Medical devices in allergy practice. World Allergy Organ J. 2020;13(10):100466–100466.
51. Edwards DA, et al. Exhaled aerosol increases with COVID-19 infection, age, and obesity. Volume 118. Proc Natl Acad Sci U S A; 2021. 8.
52. Mansour E, et al. Measurement of temperature and relative humidity in exhaled breath. Sens Actuators B. 2020;304:127371.
53. Cruickshank-Quinn C, et al. Determining the presence of asthma-related molecules and salivary contamination in exhaled breath condensate. Respir Res. 2017;18(1):57.
54. Zamuruyev KO, et al. Human breath metabolomics using an optimized non-invasive exhaled breath condensate sampler. J Breath Res. 2016;11(1):016001.
55. Czebe K, et al. Influence of condensing equipment and temperature on exhaled breath condensate pH, total protein and leukotriene concentrations. Respir Med. 2008;102(5):720–5.
56. Ma J, et al. Coronavirus Disease 2019 Patients in Earlier Stages Exhaled Millions of Severe Acute Respiratory Syndrome Coronavirus 2 Per Hour. Clin Infect Dis. 2021;72(10):e652–4.
57. Zhou L, et al. Breath-, air- and surface-borne SARS-CoV-2 in hospitals. J Aerosol Sci. 2021;152:105693.
58. Ma J, et al. Coronavirus Disease 2019 Patients in Earlier Stages Exhaled Millions of Severe Acute Respiratory Syndrome Coronavirus 2 Per Hour. Clin Infect Dis. 2020;72(10):e652–4.
59. Feng B, et al. Multi-route transmission potential of SARS-CoV-2 in healthcare facilities. J Hazard Mater. 2021;402:123771.
60. Moschos SA, Usher L, Lindsay MA. Clinical potential of oligonucleotide-based therapeutics in the respiratory system. Pharmacol Ther. 2017;169:83–103.
61. Jayaweera M, et al. Transmission of COVID-19 virus by droplets and aerosols: A critical review on the unresolved dichotomy. Environ Res. 2020;188:109819–109819.
62. Morawska L, Milton DK. It Is Time to Address Airborne Transmission of Coronavirus Disease 2019 (COVID-19). Clin Infect Dis. 2020;71(9):2311–3.
63. Majra D, et al. SARS-CoV-2 (COVID-19) superspreader events. J Infect. 2021;82(1):36–40.
64. Lemieux JE, et al. Phylogenetic analysis of SARS-CoV-2 in Boston highlights the impact of superspreading events. Science. 2021;371(6529):eabe3261.
65. Kim S, et al. Evaluation of COVID-19 epidemic outbreak caused by temporal contact-increase in South Korea. Int J Infect Dis. 2020;96:454–7.
66. Chang S, et al. Mobility network models of COVID-19 explain inequities and inform reopening. Nature. 2021;589(7840):82–7.
67. Fang Y, et al. Sensitivity of Chest CT for COVID-19: Comparison to RT-PCR. Radiology. 2020;296(2):E115–7.
68. Wikramaratna PS et al. *Estimating the false-negative test probability of SARS-CoV-2 by RT-PCR.* Euro surveillance: bulletin Europeen sur les maladies transmissibles = European communicable disease bulletin, 2020. 25(50): p. 2000568.
69. Ryan DJ, et al. Use of exhaled breath condensate (EBC) in the diagnosis of SARS-COV-2 (COVID-19). Thorax. 2021;76(1):86–8.

70. Samaddar A, et al. Viral Ribonucleic Acid Shedding and Transmission Potential of Asymptomatic and Paucisymptomatic Coronavirus Disease 2019 Patients. Open Forum Infect Dis. 2021;8(1):ofaa599.
71. Zheng S, et al. Viral load dynamics and disease severity in patients infected with SARS-CoV-2 in Zhejiang province, China, January-March 2020: retrospective cohort study. BMJ. 2020;369:m1443.
72. Malik M, et al. SARS-CoV-2: Viral Loads of Exhaled Breath and Oronasopharyngeal Specimens in Hospitalized Patients with COVID-19. Int J Infect diseases: IJID : official publication Int Soc Infect Dis. 2021;110:105–10.
73. Tinglev Å. Characterization of exhaled breath particles collected by an electret filter technique. J Breath Res. 2016;10(2):026001.
74. McDevitt JJ, et al. Development and Performance Evaluation of an Exhaled-Breath Bioaerosol Collector for Influenza Virus. Aerosol Sci Technol. 2013;47(4):444–51.
75. Bourouiba L. Fluid Dynamics of Respiratory Infectious Diseases. Annu Rev Biomed Eng. 2021;23(1):547–77.
76. Coleman KK, et al. Viral Load of Severe Acute Respiratory Syndrome Coronavirus 2 (SARS-CoV-2) in Respiratory Aerosols Emitted by Patients With Coronavirus Disease 2019 (COVID-19) While Breathing, Talking, and Singing. Clin Infect Dis. 2022;74(10):1722–8.
77. Alsved M, et al. Exhaled respiratory particles during singing and talking. Aerosol Sci Technol. 2020;54(11):1245–8.
78. Gregson FKA, et al. Comparing aerosol concentrations and particle size distributions generated by singing, speaking and breathing. Aerosol Sci Technol. 2021;55(6):681–91.
79. Asadi S, et al. Aerosol emission and superemission during human speech increase with voice loudness. Sci Rep. 2019;9(1):2348.
80. Johnson GR, et al. Modality of human expired aerosol size distributions. J Aerosol Sci. 2011;42(12):839–51.
81. Reynolds D, et al. Comprehensive Immunologic Evaluation of Bronchoalveolar Lavage Samples from Human Patients with Moderate and Severe Seasonal Influenza and Severe COVID-19. J Immunol. 2021;207(5):1229–38.
82. Bezel P, et al. Evaluation of cytokines in the tumor microenvironment of lung cancer using bronchoalveolar lavage fluid analysis. Cancer Immunol Immunother. 2021;70(7):1867–76.
83. Kowalski B, et al. Analysis of cytokines in serum and bronchoalveolar lavage fluid in patients with immune-checkpoint inhibitor-associated pneumonitis: a cross-sectional case-control study. J Cancer Res Clin Oncol. 2022;148(7):1711–20.
84. Jones KP, et al. A comparison of albumin and urea as reference markers in bronchoalveolar lavage fluid from patients with interstitial lung disease. Eur Respir J. 1990;3(2):152–6.
85. Mailhot-Larouche S, et al. Identifying Super-Responders: a Review of the Road to Asthma Remission. Ann Allergy Asthma Immunol; 2024.
86. Chen D, Bryden WA, Wood R. Detection of Tuberculosis by The Analysis of Exhaled Breath Particles with High-resolution Mass Spectrometry. Sci Rep. 2020;10(1):7647.

Figures

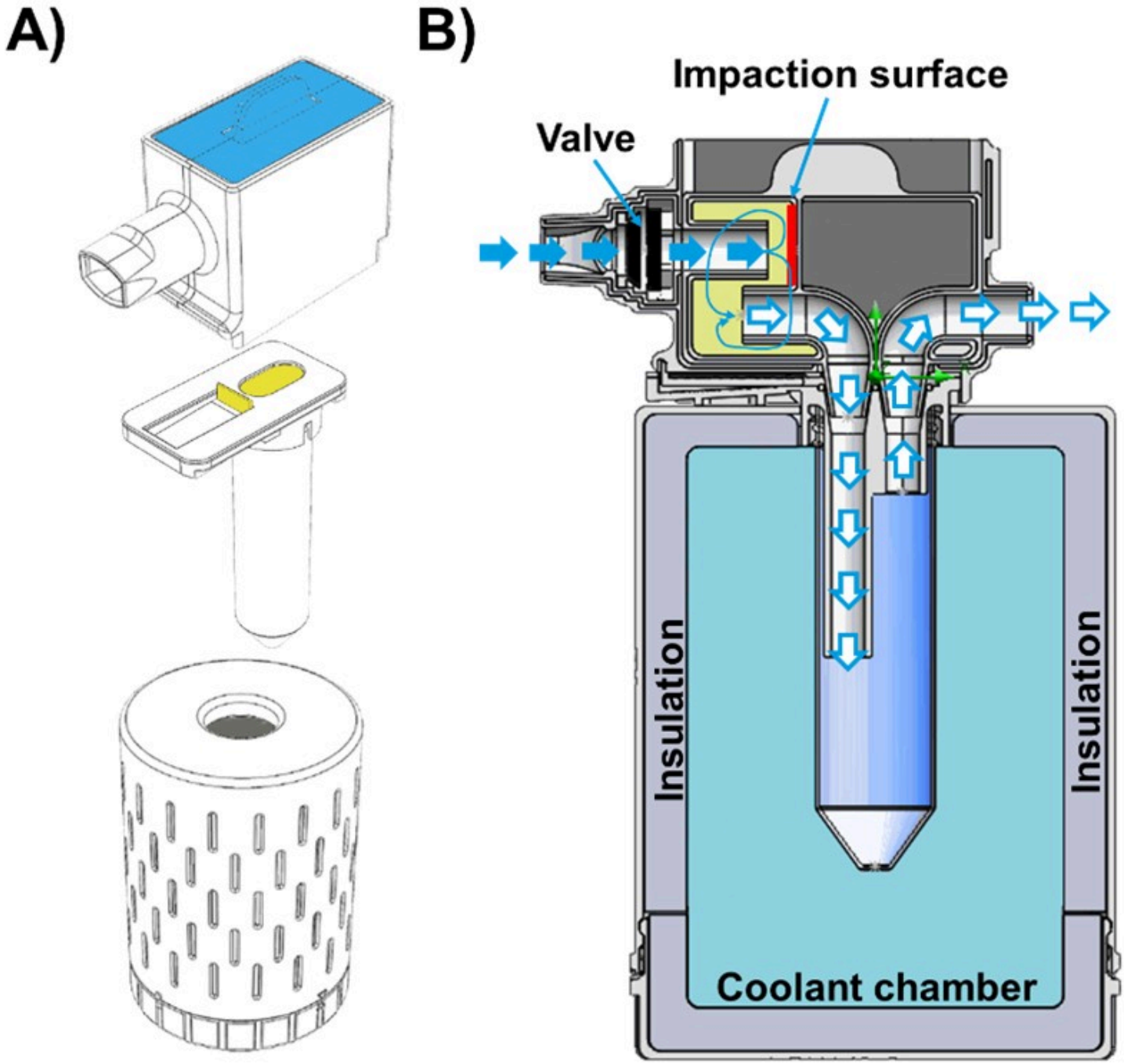


Figure 1

. The PBM-Hale™ prototype. (A) Schematic of the 3D-printed PBM-Hale^{TM} prototype showing a saliva-trapping separator with a one-way inspiratory valve (top), a 50 mL exhaled breath condensate (EBC) collection vial mounted on a self-sealing platform (middle); an insulated coolant chamber for 50mL vials is also shown (bottom). (B) Patients inhale via the nose and exhale via the separator (blue thick arrows) or into an adapted facemask coupled to the separator. The one-way valve prevents inhalation through the device. Exhaled air impacts an internal separator surface (red perpendicular line), where turbulent flow (thin blue lines) deposits

large salivary droplets in the saliva trap (yellow). Fine aerosols (FA; white arrows) then enter the collection vial (blue gradient); FA is partly condensed in the collection vial, with the uncondensed fraction exiting via an exhaust port. The vial can be immersed in coolant (cyan), for example dry ice, inside a lockable insulated container. The lockable drawer in the collection vial platform (yellow in (A)) limits ambient aerosol entry and seals the collection tube after sampling.

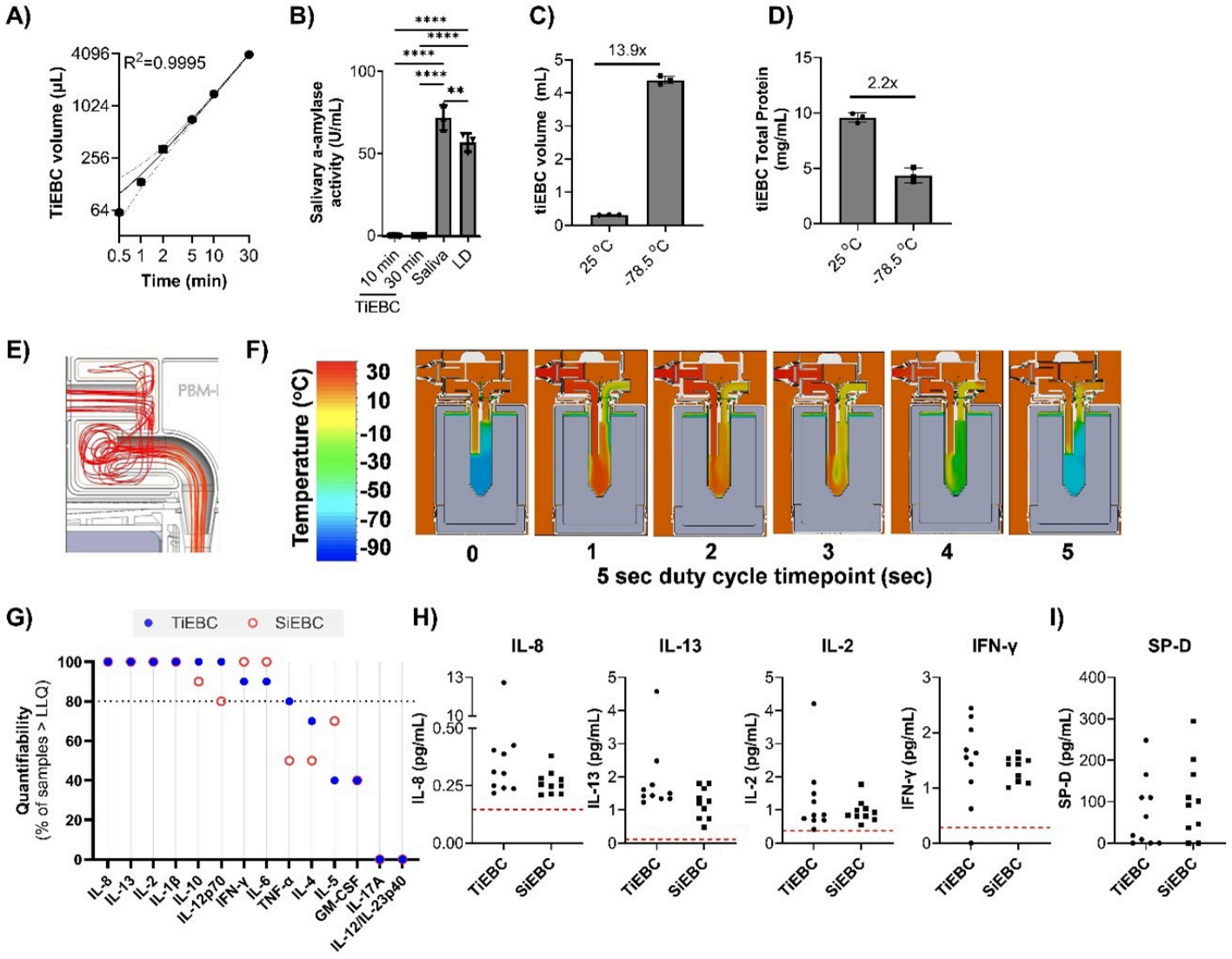


Figure 2

The PBM-Hale™ prototype reproducibly captures saliva-free and protein biomarker-rich EBC specimens from distal lungs. (A) Linear relationship between sampling time and EBC volume for tidal breathing (TiEBC; 0.5–30 minutes; n=3 samples per time point) collected at −78.5 °C. (B) Salivary alpha-amylase activity in TiEBC collected over 10 or 30 minutes of tidal breathing compared with saliva and large droplet (LD) fractions recovered from the saliva trap show no detectable salivary alpha-amylase in TiEBC (n=3-5 samples/group). (C) TiEBC volume and (D) total protein concentration after 30 minutes of sampling at different condensation temperatures (n=3/group) show that dry ice condensation markedly increases EBC volume without proportionally diluting protein content. (E,F) Computational flow and thermodynamic modelling of a 0.5 L tidal

breath duty cycle through PBM-Hale^{TM} at −78.5 °C (exhalation: 0-3 sec; inhalation: 4-5 sec) showing (E) turbulent flow fields within the saliva trap during exhalation and (F) preferential condensation within the collection vessel during the static inhalation phase. (G-I) Inflammatory markers and SP-D were quantified in EBC collected via tidal breathing (TiEBC) or singing (SiEBC) for 30 and 15 minutes, respectively; n=10 healthy study participants. (G) Proportion of EBC samples above the lower limit of quantification (LLQ) of the Mesoscale Discovery V-plex immunoassay. (H) Levels of IL-8, IL-13, IL-2 and IFN-γ and (I) SP-D in TiEBC and SiEBC. Enrichment for SP-D supports a distal airway or alveolar contribution to EBC content. Dashed red lines in (H) represent the LLQ of the immunoassay.

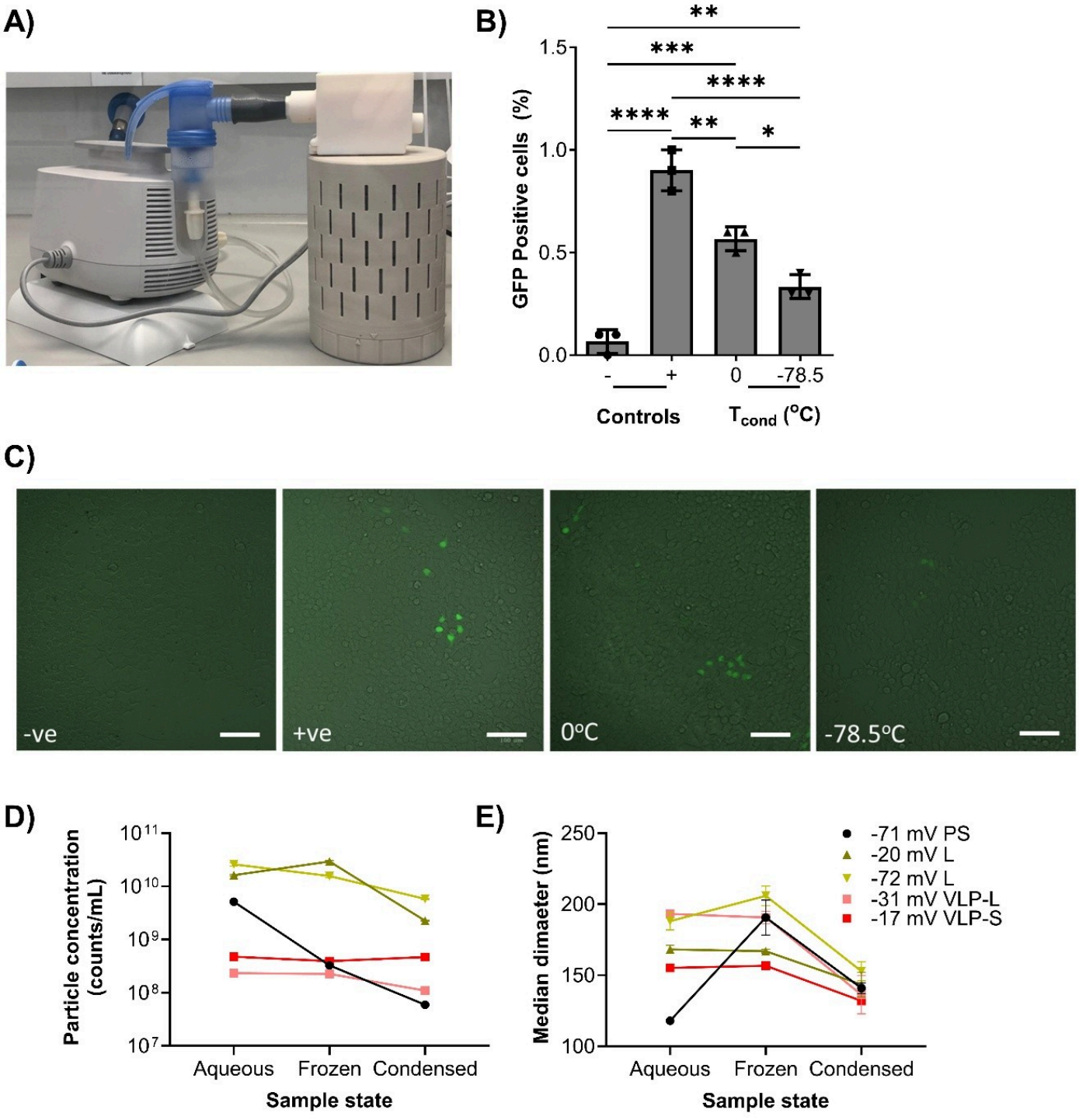


Figure 3

PBM-Hale™ FA EBC enables viral aerosol capture. (A-C) VSV-G pseudotyped GFP-encoding lentivirus was mechanically nebulized though PBM-Hale™ cooled at 0 °C or -78.5 °C as shown in (A). Virion condensates were incubated with HEK293T cells and the resulting GFP fluorescence assessed either via (B) flow cytometry or (C) fluorescence microscopy. Direct cell transduction with the VSV-G pseudotyped, GFP-encoding lentivirus suspension (positive control; +ve) or incubation with vehicle (autofluorescence; negative control; -ve) were used as controls. (B) Percentage of GFP positive HEK293T cells and (C) representative microscopy images are shown. (D-E) Effect of flash-freezing or mechanical aerosolization/condensation capture of polysterene beads (PS), liposomes (L), lentiviral virus-like particles (VLP-L), or SARS-CoV-2 virus-like particles (VLP-S) on (D) particle concentration and (E) median diameter, as measured by nanoparticle tracking analysis (mean ± SD of 3 independent replicates). The net zeta potential (charge) of each particle type is shown. *: $p<0.05$; **: $p<0.01$; ***: $p<0.001$; ****: $p<0.0001$.

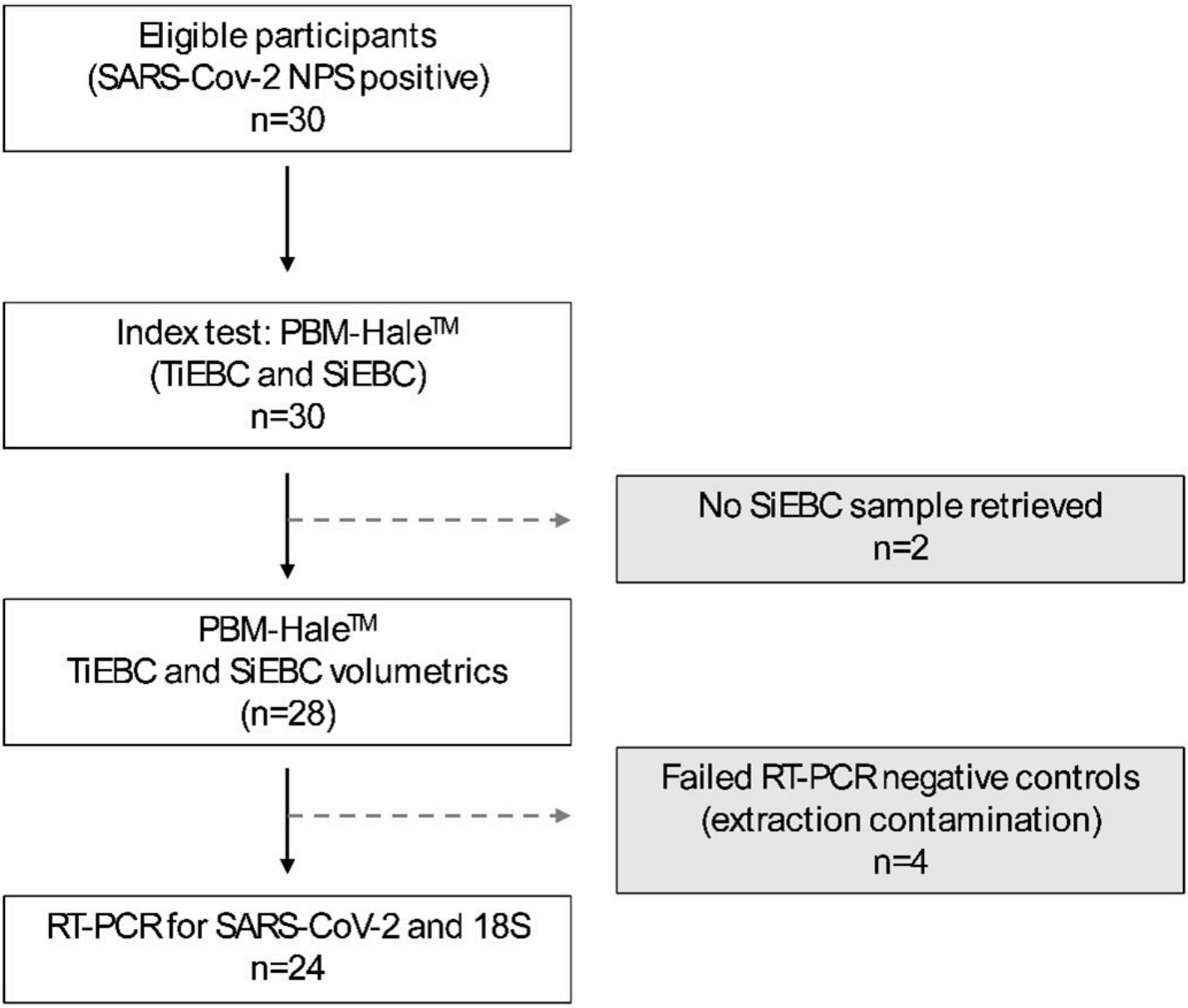


Figure 4

Schematic overview of the study. NPS= Nasopharyngeal swab. TiEBC = Exhaled breath condensate collected via tidal breathing. SiEBC = Exhaled breath condensate collected via a singing maneuver.

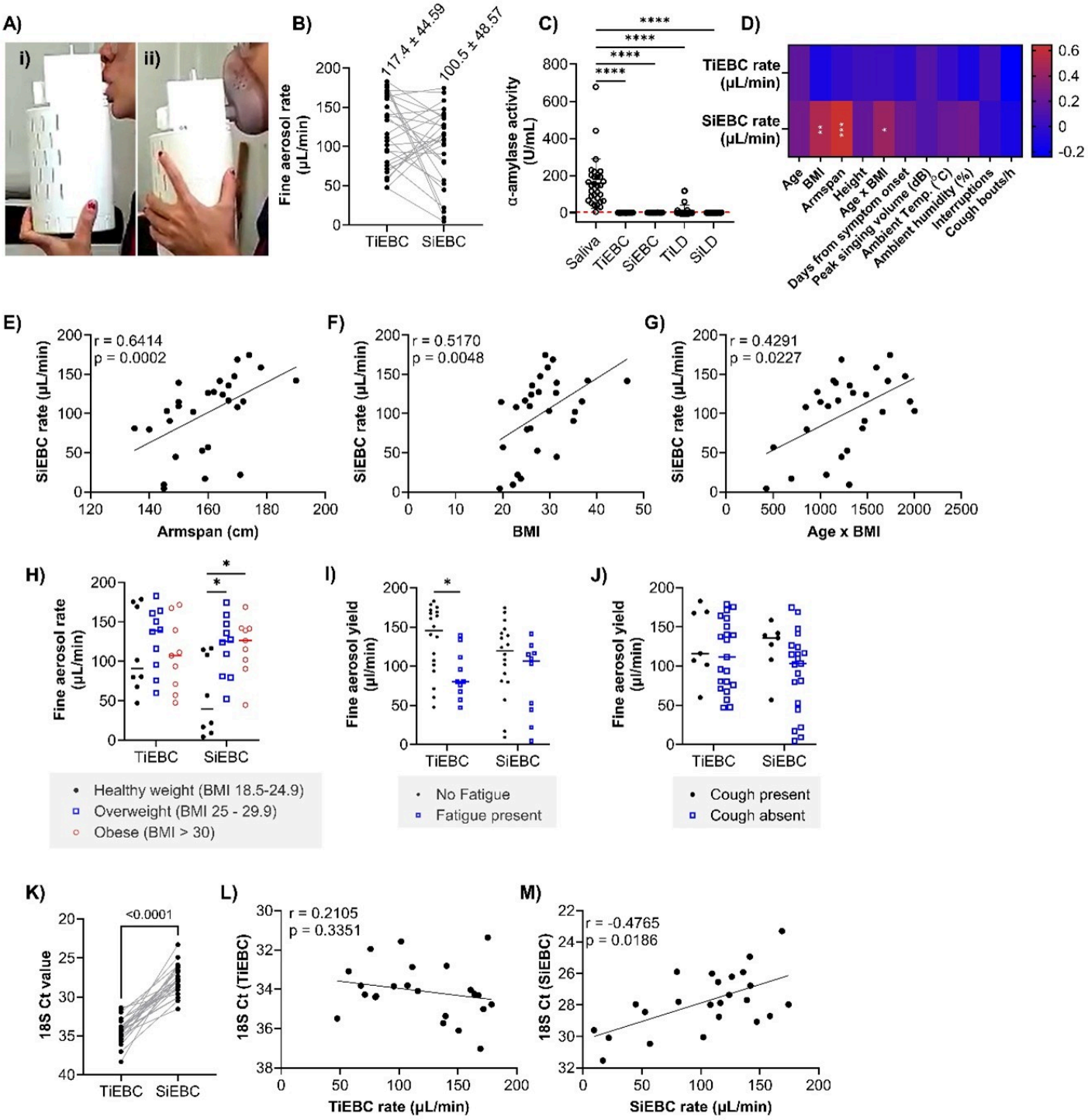


Figure 5

Properties of distal lung FA EBC collected by tidal breathing or singing from COVID-19 patients using PBM-Hale™ under dry ice condensation. COVID-19 NPS-positive patients (n = 30) provided FA EBC by tidal breathing for 30 minutes (TiEBC) or by singing “Happy Birthday” in Portuguese for 15 minutes (SiEBC) into the PBM-Hale^{TM} prototype. The coolant chamber was loaded with dry ice for -78.5 °C fine aerosol condensation. Twenty-eight of the 30 participants generated sufficient EBC volume for downstream analysis. (A) Representative images of FA EBC collection with PBM-Hale^{TM} via (i) oral tidal breathing and (ii) singing. For SiEBC, PBM-Hale^{TM} was coupled to a one-way valve facemask ensuring ambient air inhalation via the mask. (B) Sampling yield rate (µL FA EBC per minute) for TiEBC and SiEBC; no significant difference between manoeuvres; n=28 (Wilcoxon matched-pairs signed rank test; p=0.2946). (C) Salivary alpha-amylase activity measured in FA EBC and in large droplet (LD) fractions recovered from the separator during tidal breathing (TiLD) and singing (SiLD). Alpha-amylase is detectable only in LD fractions, confirming separation of saliva-containing LD from FA EBC. Dotted red line indicates the LLQ of the assay; **** p < 0.0001 by Kruskal–Wallis test followed by Dunn’s multiple comparisons test (all groups *vs* saliva). (D) Spearman correlation heatmap of TiEBC and SiEBC sampling rates with anthropometric variables, days since symptom onset (0–5 days), ambient temperature and humidity, singing volume, cough bouts per hour, and number of interruptions during sampling. Positive correlations (red) are observed for SiEBC, but not TiEBC, between sampling rate and (E) armspan (r = 0.6414, ***p = 0.0002), (F) BMI (r = 0.517, **p = 0.0048) and (G) age × BMI (r = 0.4291, *p = 0.0227). (H) EBC sampling rate according to BMI category; SiEBC, but not TiEBC rate is increased in overweight (BMI 25–29.9) and obese (BMI > 30) COVID-19 patients compared with normal weight (*p < 0.05; 2-way ANOVA). (I) Effect of self-reported fatigue on TiEBC and SiEBC sampling rates (n = 28); fatigue reduces TiEBC but not SiEBC yield (p = 0.2946 for SiEBC, 2-way ANOVA). (J) Effect of presence/absence of cough on FA yields. (K) 18S RNA Ct values in TiEBC and SiEBC specimens; Wilcoxon paired non-parametric t-test. (L-M) 18S rRNA levels (RT-PCR Ct values), quantified by pan-eukaryotic TaqMan 18S rRNA assay, expressed as a function of FA EBC sampling rate during (L) TiEBC and (M) SiEBC.

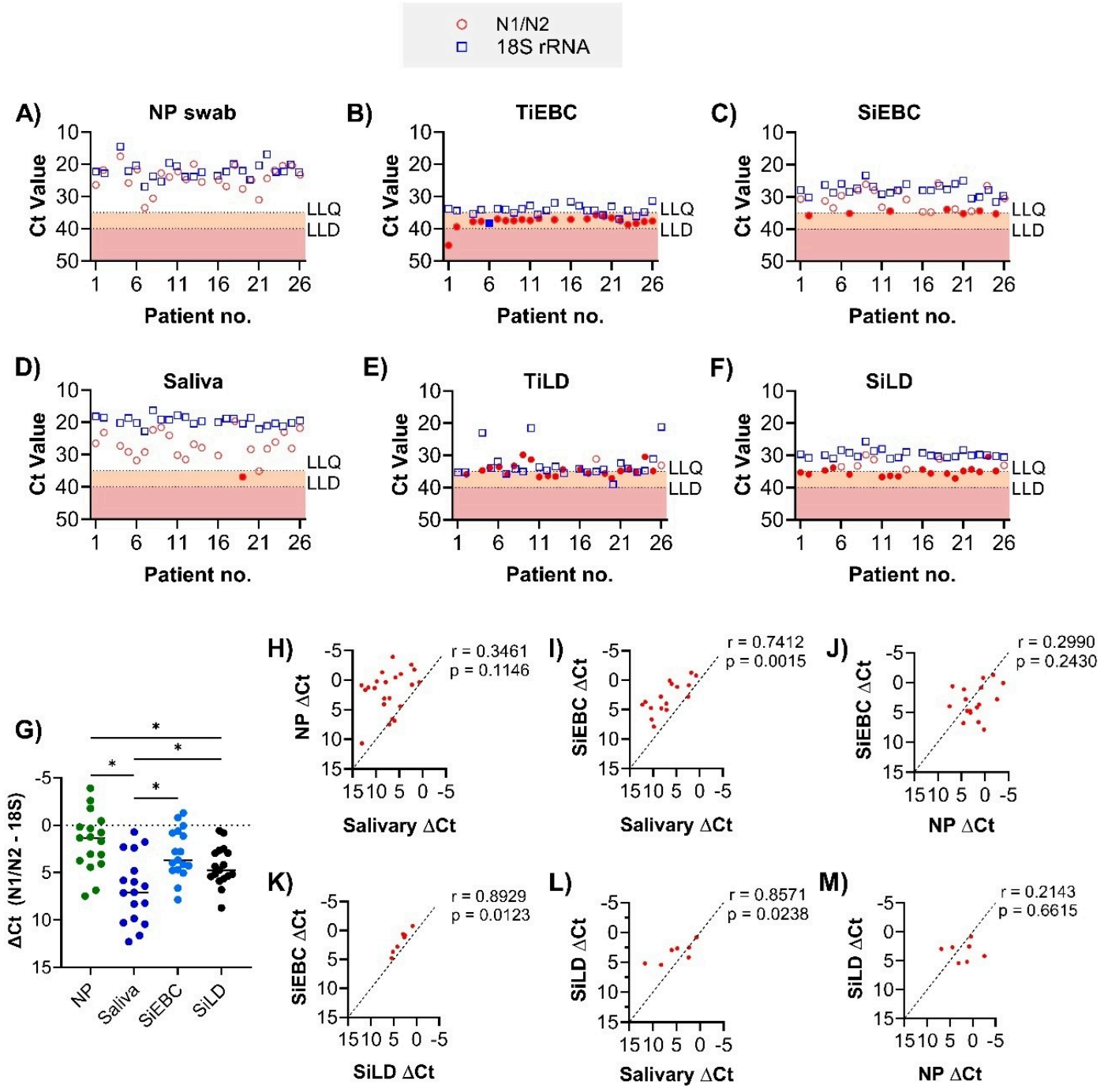


Figure 6

Singing increases 18S rRNA and SARS-Cov-2 RNA loads in distal lung breath condensate collected with PBM-Hale™, to reveal higher pulmonary viral RNA levels specific to the lung within 5 days from symptom onset. (A-F) Total RNA (18S rRNA) and SARS-CoV-2 RNA (N1/N2) in COVID-19 patient specimens collected in days 0-5 from symptom onset, expressed as Ct values (n=24). (A) Nasopharyngeal swab (NPS) and (D) saliva samples were collected prior to (B) tidal EBC (TiEBC) and (C) singing EBC (SiEBC) sampling. (C, F) Large droplets (LD) retrieved by washing the saliva trap with 0.2mL of PBS. All RT-PCR reactions in triplicate. Solid symbols indicate samples where at least one out of three RT-PCR replicates did reach the lower limit of detection (LLD; Ct ≤ 40). Open symbols: all three RT-PCR replicates resulted in Ct values above the LLD (Ct ≤

40). LLQ: lower limit of quantification (Ct=35). All samples were processed in 3 batches. Samples 3 and 15 excluded due to absence of any SiEBC volume recovery. Samples 27-30 excluded due to extraction-related contamination detected by 18S rRNA negative control positivity occurring in siEBC specimen processing, but not alternative specimens. (G) SiEBC have comparable normalized viral loads (ΔCt = N1/N2 average Ct – 18S Ct) to NP and SiLD, but higher than saliva. (H-M) Non-parametric Spearman correlations of 18S rRNA-normalized viral loads between paired samples with a positive SARS-Cov-2 PCR (3/3 replicates Ct<40 for both N1 and N2). Graphs indicate correlations between EBC sampled by singing (SiEBC) versus saliva, n=16 (I), or singing droplets (SiLD), n=7; K) but not NP swabs, n=17 (J). SiLD viral loads correlate with salivary (L), but not NP swab viral loads (M), L-M n=7 pairs; no correlation between NP swab and salivary viral loads, n=22 pair of samples (H). Diagonal dotted line in graphs H-M indicates no difference in normalised viral load between DCt values from each pair of specimens; points to the left of the dotted line indicate higher level in Y axis specimens.

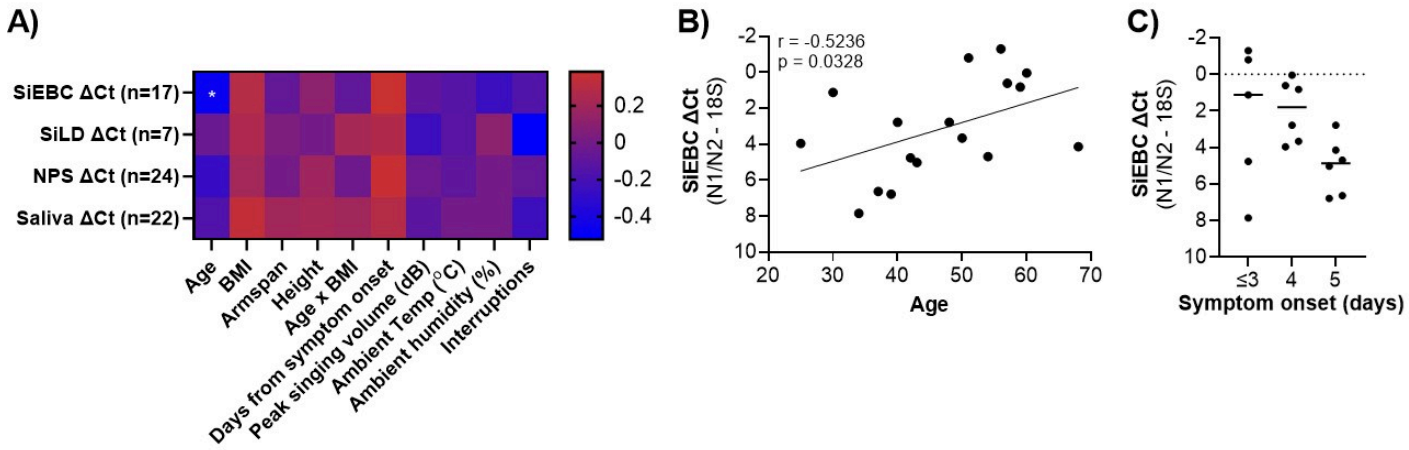


Figure 7

SARS-Cov-2 viral loads in EBC obtained via singing increase with age. (A) Spearman correlation heatmap of normalised SARS-CoV-2 viral loads (ΔCt = N1/N2 Ct – 18S Ct) measured in singing-derived EBC (SiEBC), large droplets recovered from the saliva trap during singing (SiLD), nasopharyngeal swabs (NPS), and saliva samples. Variables tested included anthropometric parameters, days since symptom onset (0–5 days), ambient temperature and humidity, singing intensity, cough bouts per hour, and sampling interruptions. Positive correlations are shown in red; a significant positive association between SiEBC viral load and age is observed. (B) ΔCt values (N1/N2 Ct – 18S Ct) for SiEBC samples plotted against age. In A-C, only SARS-CoV-2–positive samples (3/3 RT-PCR replicates positive for N1 or N2) were included in the analysis.

Supplementary Files

This is a list of supplementary files associated with this preprint. Click to download.

- 16APR2026COVEXHALESupplementaryMethods.docx
- Video1.mp4
- Supplementary.docx